Newsletters on Stratigraphy
Published online September 2016

PrePub Article

Astronomical tuning of the La Vedova section between 16.3 and 15.0 Ma. Implications for the origin of megabeds and the Langhian GSSP

Elena Turco[1]*, Silja Hüsing[2], Frederik Hilgen[3], Antonio Cascella[4], Rocco Gennari[1], Silvia Maria Iaccarino[1], and Leonardo Sagnotti[5]

With 12 figures and 3 tables

Abstract. The early–middle Miocene, marked by the Middle Miocene Climatic Optimum (MMCO) followed by the Middle Miocene Climate Transition (MMCT) towards cooler temperatures, represents a crucial period in Earth's climate evolution. To understand this episode and reconstruct its origin and the regional impact of the observed global changes, it is critical that high-resolution astronomical age models are developed for climate sensitive regions around the world. One of these areas undoubtedly is the Mediterranean, but so far no such an age model has been established for the interval of the MMCO. Nevertheless, this interval is well exposed in the coastal cliffs along the Adriatic Sea near Ancona (Italy), where it is characterized by the occurrence of 7 conspicuous limestone beds, termed megabeds, alternating with marl intervals. Here, we use the Lower La Vedova Beach section to construct an astronomical time scale for the younger part of the MMCO in the Mediterranean. The tuning to ~100-kyr eccentricity seems robust, but is less certain for precession in some intervals, as a consequence of the less clearly developed internal structure of the basic precession related cycles and uncertainties in the phase relation with climatic precession and insolation and in the astronomical solution in terms of tidal dissipation and dynamical ellipticity values. The tuning nevertheless provides astronomical ages for calcareous plankton events and magnetic reversals for the interval between 16.3 and 15.0 Ma. Individual megabeds are related to the ~100-kyr eccentricity cycle corresponding to eccentricity minima and the megabed interval itself is partly controlled by the 405-kyr cycle, as it marks two successive minima and the maximum in between. However, no relation with very long period eccentricity cycles (2.4 and 1 myr) is evident, and a link to regional tectonic processes (a major orogenic phase at the base of the Langhian and the likely associated Langhian transgression) seems more plausible. The higher sedimentation rate in the megabeds can be explained by the additional preservation of biogenic silica, which may also account for the diluted planktonic foraminiferal assemblages. With the integrated magnetobiostratigraphy and the tuning to eccentricity and to precession/insolation, the Lower La Vedova Beach section meets key requirements for defining the Langhian GSSP.

Key words. Burdigalian/Langhian boundary, magnetobiostratigraphy, element geochemistry, astronomical tuning, Mediterranean, environmental changes

Authors' addresses:
[1] Dipartimento di Fisica e Scienze della Terra, Università di Parma, Parco Area delle Scienze 157/A, 43124 Parma, Italy.
[2] Paleomagnetic Laboratory ‚Fort Hoofddijk', Utrecht University, Budapestlaan 17, 3584 CD Utrecht, The Netherlands.
[3] Department of Earth Sciences, Utrecht University, Heidelberglaan 2, 3584 CS Utrecht, The Netherlands.
[4] Istituto Nazionale di Geofisica e Vulcanologia (INGV), Via della Faggiola 32, 56126 Pisa, Italy.
[5] Istituto Nazionale di Geofisica e Vulcanologia (INGV), Via di Vigna Murata 605, 00143 Roma, Italy.
* Corresponding author: elena.turco@unipr.it

DOI: 10.1127/nos/2016/0302

www.borntraeger-cramer.de
0078-0421/2016/0302 $ 7.25

1. Introduction

The early–middle Miocene represents a crucial period in Earth's climate evolution and is characterized by the Middle Miocene Climatic Optimum (MMCO) between ~17 and ~15 Ma. This climatic optimum is followed by a gradual decline in temperature during the Middle Miocene Climate Transition (MMCT) between 15 and 14 Ma, culminating in the marked Mi 3b oxygen isotope increase at 13.8 Ma that supposedly reflects rapid growth of the East Antarctic Ice Sheet (Miller et al. 1991, Abels et al. 2005, Holbourn et al. 2005, 2013, 2014). In addition, the middle Miocene is characterized by the Monterey carbon isotope excursion, which started at ~17 and ended at ~13.5 Ma approximately 300 kyr after the major expansion of the Antarctic ice-sheet (Vincent and Berger 1985, Woodruff and Savin 1991, Holbourn et al. 2007). This long lasting positive carbon isotope excursion corresponds to an episode of enhanced burial of organic matter and consists of nine 400 kyr cycles showing high coherency with long eccentricity (Holbourn et al. 2007). To disentangle this intricate global climate history, high-resolution astronomically calibrated time scales are essential. For the middle Miocene, such a time scale is already available for the open ocean, with high-resolution benthic foraminiferal isotope records providing highly valuable insights in the pattern of global climate change during this period (Holbourn et al. 2005, 2007, 2013, 2014, Tian et al. 2013).

To understand the origin and regional expression of the MMCO and MMCT, it is essential that similar high-resolution time scales and proxy records are established for climate sensitive regions. One of these areas undoubtedly is the Mediterranean, which is well known to record the impact of both global and regional climate change and, in turn, may have influenced global climate variation through changes in gateway configuration affecting ocean circulation. Up to now, a tuned time scale has been established for the MMCT in the Mediterranean (Hüsing et al. 2010, Mourik et al. 2010), showing that the deposition of the oldest dark organic-rich layers termed sapropels directly postdate the Mi 3b cooling event. However, a similar high-resolution time scale is lacking for the MMCO. Integrated magnetobiostratigraphic records have recently been published from several Mediterranean sections, including La Vedova in northern Italy (Turco et al. 2011a) and St. Peter's Pool on Malta (Foresi et al. 2011), which are potentially suitable for astronomical tuning.

Here, we will focus on the astronomical tuning to eccentricity and precession/insolation of the La Vedova section of Turco et al. (2011a), which represents the downward extension of the La Vedova Beach section of Hüsing et al. (2010). In this study, we refer to this extension as the Lower La Vedova Beach section to distinguish it from the (Upper) La Vedova Beach section of Hüsing et al. (2010). The Lower La Vedova Beach section is marked by the occurrence of prominent megabeds (Sandroni 1985, Montanari et al. 1997), which may represent the local expression of the MMCO in the Mediterranean between 16.3 and 15.0 Ma. At the same time, it is presented as one of the candidate sections for the formal definition of the Langhian Global Stratotype Section and Point (GSSP) (Turco et al. 2011a, Iaccarino et al. 2011).

2. Geological setting and section

The Lower La Vedova Beach section is exposed along the coastal cliffs 3 km southeast of Ancona (Italy) (Fig. 1) and can be reached via steep paths going down the cliffs from La Vedova village or by boat. The section represents the downward extension of the Upper La Vedova Beach and La Vedova High Cliff sections documented by Hüsing et al. (2010) and Mourik et al. (2010), respectively, and astronomically dated between ~15 and 13.5 Ma. The entire La Vedova section belongs to the lower portion of the Schlier Formation, a (hemi)pelagic unit deposited in the eastern part of the Umbria-Marche basin, which formed part of the external domain of the NE verging thrust belt of the Apennine orogen (for more details see Montanari et al. 1997). In particular, the investigated section belongs to the Massive Member of the Schlier Formation and includes the megabeds described by Sandroni (1985) as "7 composite but apparently massive layers of hemipelagic marls". According to Montanari et al. (1997), the top of this member coincides with the Aldo level, an ash-bed that is located higher in the succession about 3 m above the top of our section in the lower part of the Upper La Vedova Beach section of Hüsing et al. (2010). The Lower La Vedova Beach composite section and the high-resolution integrated magnetobiostratigraphy were published by Turco et al. (2011a). However, much improved outcrop conditions after severe winter storms during 2011 and 2012 (Fig. 2; Supplementary material A, Fig. A1) led to a more accurate description of the lithology and revealed the presence of a fault in the megabed interval in the lower part of

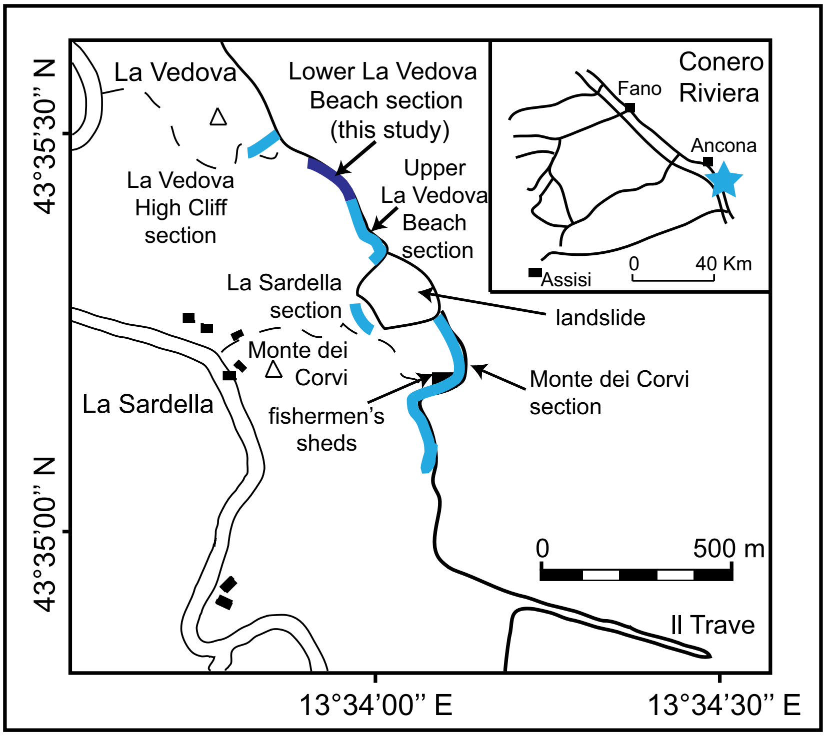

Fig. 1. Location map for the Lower La Vedova Beach section.

the section. The offset of this fault was determined by means of detailed stratigraphic correlations and the resulting modified log and magnetobiostratigraphic record are used as starting point for the present paper (see Results).

3. Material and methods

3.1 Lithology

The lithologic log of Turco et al. (2011a) has been modified by taking into account the higher quality of the exposures following the winter storms and the revised adjustment across the fault. Apart from adding the missing interval, the log itself was also modified paying special attention to the expression of the individual marly and more calcareous intervals on the scale of the megabeds. The megabeds that are present in the lower part of the section are numbered from I to VII following the codification of Sandroni (1985) and Montanari et al. (1997). Above this interval we could recognize 6 additional indurated intervals and decided to extend the numbering on the megabed scale to the top of the section, but displaying the roman numerals (VIII–XIII) in italics to distinguish them from the real megabeds (I–VII) in bold. Next to the lithologic column, the fresh color of the small hand-drilled cores of the samples is shown, which is based on the comparison of wet color of the cores with the Rock Color Chart (Goddard et al. 1963). This comparison was previously described in Turco et al. (2011a), who distinguished intercalations of greenish gray levels (5.0 GY 6/1), and more rarely light olive gray (5.0 Y 5/2) and light bluish gray (5.0 B 7/1), within the predominant olive gray (5.0 Y 4/1) sediments.

3.2 Calcareous plankton

The planktonic foraminiferal and calcareous nannofossil data set of Turco et al. (2011a) was enlarged by analyzing extra samples taken from the better exposed left side of the fault in order to determine its offset. The planktonic foraminiferal data set was further enlarged by adding samples from all the sediment color alternations present in the section in an attempt to find a relationship between species abundance and lithology. In total 330 samples were analyzed; however, the semi-quantitative methodology described in Turco et al. (2011a) was applied only on 239 samples because of the poor preservation (mainly in limestone layers) or the scarcity of planktonic foraminifera (mainly in the megabeds).

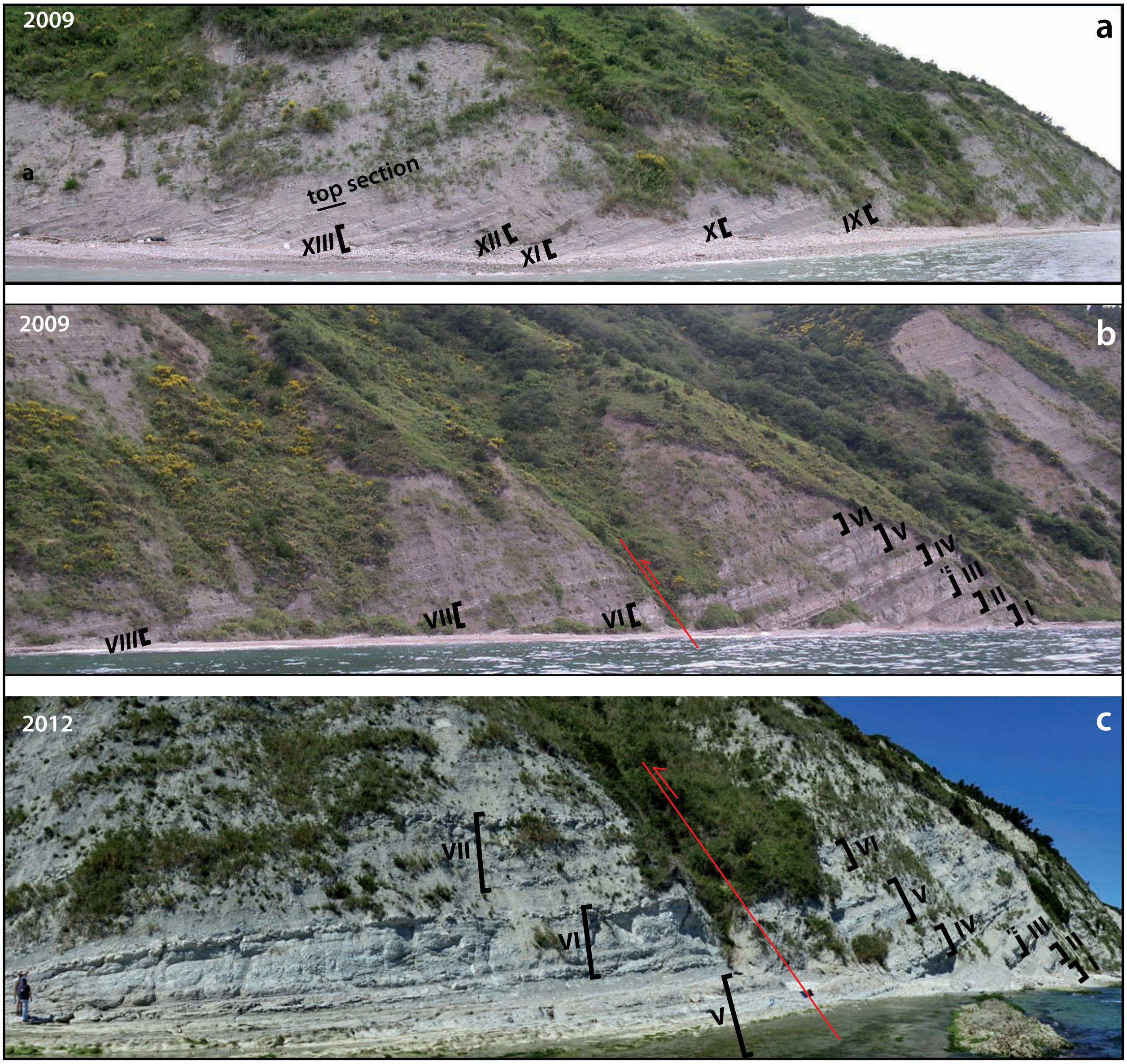

Fig. 2. Photographs of the Lower La Vedova Beach section showing: a) the upper part from Megabed IX to the top; b and c) the lower part from the base (Megabed II) to Megabed VIII. The improvement in the quality of the exposure between summer 2009 (b) and summer 2012 (c) led to the determination of the fault offset and to the revised correlation of megabeds (see also text and Supplementary material A).

3.3 Magnetostratigraphy and geophysical proxy (MS)

Extra samples were taken from the better exposed left side of the fault in order to complete the magnetostratigraphic record of the section. The magnetic susceptibility (MS) of 566 samples was measured on a Kappabridge KLY-2 and their weight on a Sartorius RC 210 P. The specific magnetic susceptibility (m^3/kg) was calculated by dividing the volume specific magnetic susceptibility of the sample by its density.

3.4 Geochemical proxies (XRF analysis)

The geochemical data were obtained by measuring the elemental composition of 566 samples, using a NITON XL3t 900Analyzer with GOLDD Technology, placed in a Thermo Scientific portable test stand. The samples were measured in Cu/Zn Mining Mode (Filters: Main 30, Low 30, High 30 and Light 60 seconds), with 2 control samples (NIST2780 and NIST2709a) measured every 9 samples. The elements measured with these settings are Zr, Sr, Fe, Al, Ca, Ti, Ba, Si, Mg, K, Nb, Rb, Zn, Mn, V, Cl and S. A helium purge was used to obtain more accurate measurements for the lighter elements (Mg, Al, Si, S). Homogeneous control samples were included in the measurements to detect possible internal fluctuations related to the measuring equipment.

Analysis was done on a flat surface to prevent that unevenness of the sample disturbs the measurements, thereby reducing their accuracy. All measurements were repeated three times at different spot positions to correct for sample inhomogeneity; these measurements were averaged to significantly reduce its effect and increase precision. Measurements were rejected and, if necessary, repeated, if the standard deviation was too high compared to the measured value (> 1.5 times 2σ).

The $CaCO_3$ content is calculated by multiplying the measured Ca concentration with a factor 2.496, assuming that all Ca present is bound by carbonate. The $CaCO_3$ content is presented in ppm, where 1 million ppm represents 100 % $CaCO_3$.

Elemental proxy records were obtained by normalizing the measured element with Al to correct for the detrital fraction (in case of redox-sensitive and chalcophilic elements, such as V and Mo, and carbonate) and to reveal subtle differences in concentrations that are not related to variation in clay content (in case of terrestrial elements such as Fe, Ti and Zr) (e.g., Nijenhuis et al. 1996, Schenau et al. 1999). An exception is the calculated Rb/Sr ratio.

3.5 Statistic and Time series analyses

An Independent Student t Test was applied to selected planktonic foraminiferal taxa and geochemical elements in order to test if their variability is related to changes in sediment color. This analysis is based on the comparison between mean values of the faunal and geochemical proxies in two different main sediment colors (greenish gray and olive gray). A Principal Component Analysis was performed on the elemental records normalized to Al in order to reduce the variability in the geochemical data set.

Wavelet analysis was applied using the Torrence and Compo (1998) guide to detect changes in the frequency-time domain that result from changes in sedimentation rate. The Blackman-Tukey method in Analyseries (Paillard et al. 1996) was used for spectral analysis in combination with bandpass filtering of the main frequency components.

4. Results

4.1 Revised composite section and magnetobiostratigraphy of the Lower La Vedova Beach section

The modified lithologic log of Turco et al. (2011a) is shown in Figures 2 and 3, and in Figures A1 and A2 of Supplementary material A. Determining the offset of the fault detected in the megabed interval was difficult in the field and, in addition, was beyond the resolution of the calcareous plankton zonations and magnetostratigraphy as it falls within the planktonic foraminiferal Subzone MMi 4a, the calcareous nannofossil Subzone MNN4b and Chron C5Br (Turco et al. 2011a). However, extra samples for biostratigraphic analysis taken from the better exposed left side of the fault allowed us to check this offset; the quantitative distribution pattern of selected calcareous plankton marker species (*Globoturborotalita woodi*, *Globoquadrina dehiscens* and *Helicosphaera ampliaperta*) in the critical interval on both sides of the fault indicates that one megabed is missing in the composite section of Turco et al. (2011a) (Fig. 3). A comparison of the internal pattern of the megabeds on both sides of the fault with the pattern observed in the cliffs just south of Ancona, where the 7 megabeds are very well exposed in an undisturbed succession, suggests that the missing megabed is Megabed VI according to the numbering introduced by Montanari et al. (1997) (Supplementary material A, Fig. A2). This is confirmed in detail by an abundance peak of *G. dehiscens*, which is found close to the top of Megabed VI and the presence of two newly detected ash layers above the same megabed both at La Vedova and in the cliffs near Ancona (Fig. 3; Supplementary material A, Fig. A2). The detection of the extra megabed in the succession and extra sampling for magnetostratigraphy and biostratigraphy resulted in a revised composite stratigraphic section and magnetobiostratigraphic record, which compensates for the missing interval (Fig. 4). The modified log and magnetobiostratigraphic record are used as starting point for the present paper (Fig. 4). On the basis of the updated magnetobiostratigraphic record, age calibrations of calcareous plankton events have been recalculated and compared with those previously published by Turco et al. (2011a) (Table 1).

4.2 Lithology

The new composite section of the Lower La Vedova Beach section is about 63 m thick and starts with

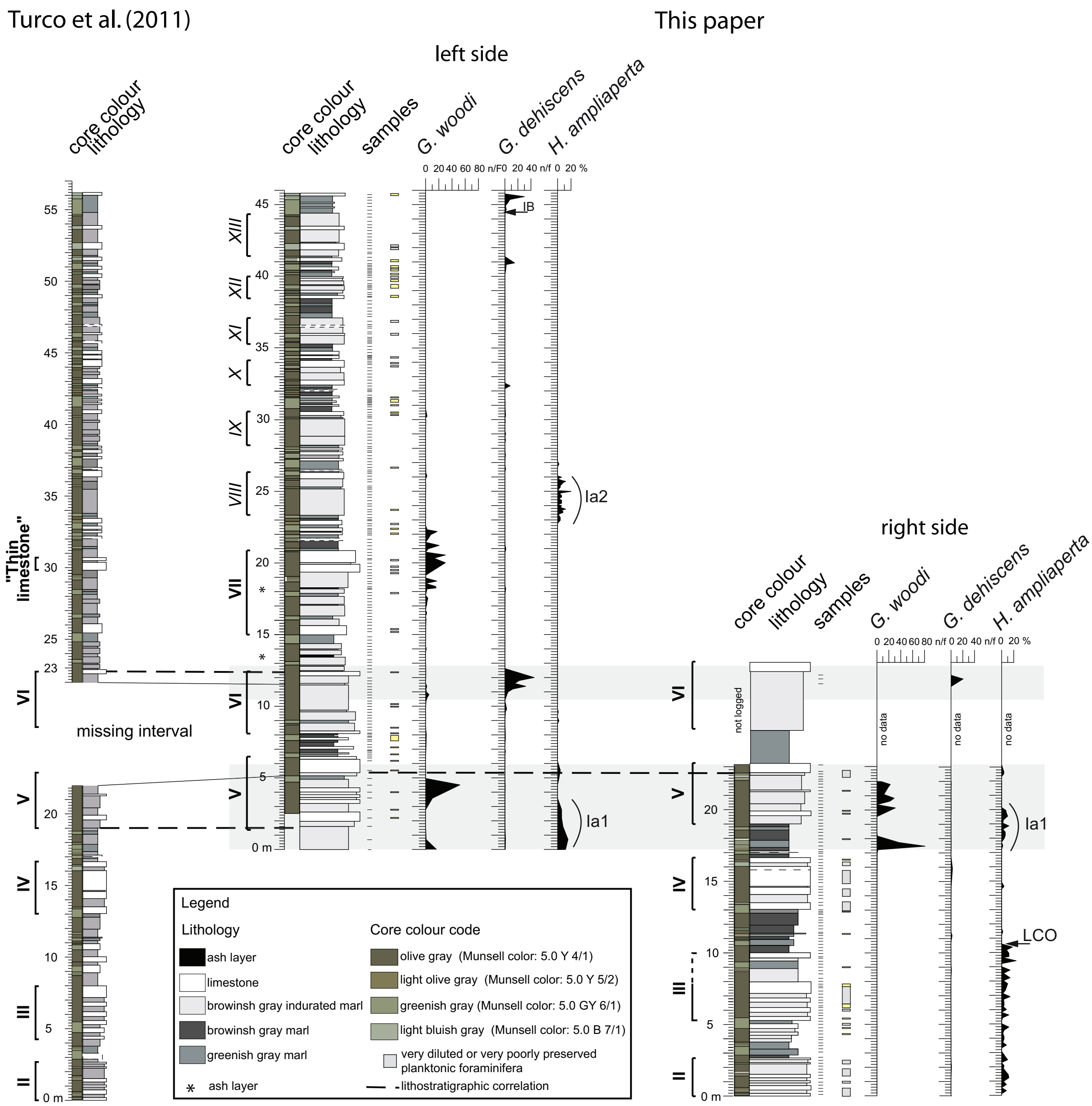

Fig. 3. Biostratigraphic correlation of the megabed interval between the two sides of the fault, that underlies the new composite used in the present study, and comparison of the improved logs of the Lower La Vedova Beach on both sides of the fault (this paper) with the previous log published in Turco et al. (2011a).

Megabed II (Figs. 2 and 4), as Megabed I was not sampled because of poor outcrop conditions. The lower 38 m of the section are characterized by Megabeds II to VII, which are separated by less indurated marl intervals. This large scale alternation of indurated limestone intervals and marls continues well above Megabed VII despite the more marly character of the succession; from 38 m up to the top of the section 6 additional indurated intervals (Megabeds VIII to XIII) can be observed. The marl intervals between megabeds are characterized by intercalations of brownish or greenish gray marls and limestone layers (less prominent and thick than in the megabed intervals) and correspond mostly to the clustering of the greenish gray layers based on the description of the fresh core color. These marl intervals are generally distinct, except for

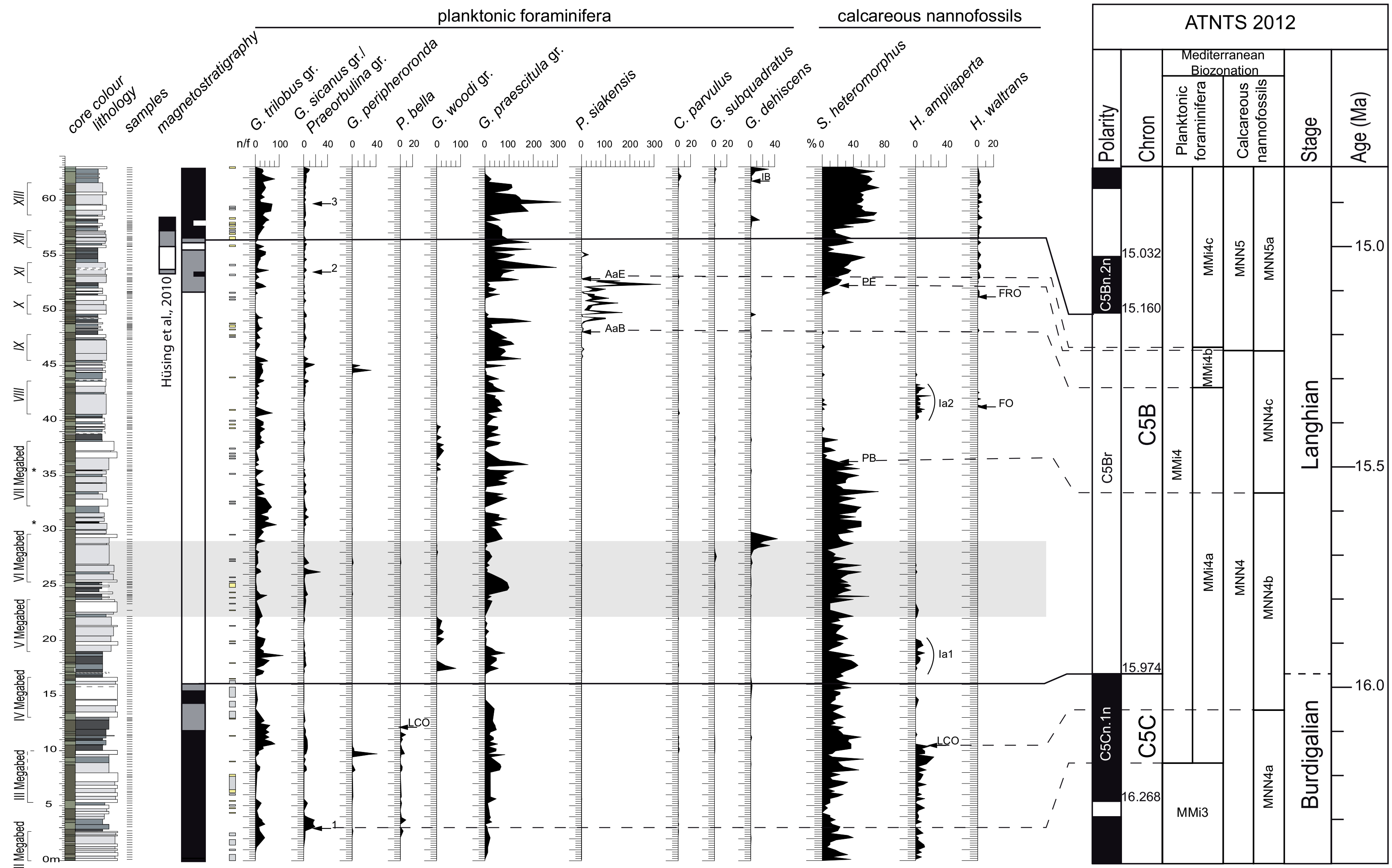

Fig. 4. The revised composite lithological column and the color record of the Lower La Vedova Beach section with the magnetostratigraphy and the distribution pattern of the calcareous plankton marker species. The gray band indicates the missing interval in the composite section of Turco et al. (2011a). The stratigraphic position of calcareous plankton events is shown beside the distribution patterns; numbers 1, 2 and 3 indicate the First Occurences (FOs) of *Globigerinoides sicanus* (3 apertures), *Praeorbulina glomerosa curva* and *P. glomerosa glomerosa*, respectively. The magnetobiostratigraphic record is correlated to ATNTS2012 and the Mediterranean biozonations of Iaccarino and Salvatorini (1982) and Iaccarino (1985) for planktonic foraminifera and of Fornaciari et al. (1996) for calcareous nannofossils, both emended in Di Stefano et al. (2008). The planktonic foraminiferal MMi 3/MMi 4 zonal boundary, identified by the FO of *Globigerinoides sicanus* (3 apertures) in the Mediterranean, was emended in Iaccarino et al. (2011).

Table 1 Comparison between the revised stratigraphic position of the magnetic reversals and average sedimentation rates in the Lower La Vedova Beach section (this paper) and those of Turco et al. (2011a). Comparison between the revised stratigraphic position, magnetostratigraphic position and calibration of the calcareous plankton events in the Lower La Vedova Beach section (this paper) and those of Turco et al. (2011a). Δ indicates the age difference of bioevents between Turco et al. (2011a) and the present paper. Magnetostratigraphic position and calibration of the calcareous plankton events in the Lower La Vedova Beach section are compared with those at DSDP Site 372 (Balearic Basin).

Lower La Vedova Beach section							
Magnetic reversal boundaries		hypothesis b_ Turco et al. 2011			hypothesis b_ This paper		
	ATNTS 2012 (Ma)	Strat. interval (m)	Mean strat. position (m)	Average sed. rate (cm/kyr)	Strat. interval (m)	Mean strat. position (m)	Average sed. rate (cm/kyr)
C5Bn.2n (y)	15.032	57.16 – 57.58	57.370 ± 0.210	C5Bn.2n: 6.035 ± 0.363	63.95 – 64.37	64.160 ± 0.210	C5Bn.2n: 6,074 ± 0.402
C5Bn.2n (o)	15.160	49.39 – 49.90	49.645 ± 0.255	C5Br: 4.165 ± 0.063	56.08 – 56.69	56.385 ± 0.305	C5Br: 4.986 ± 0.075
C5Cn.1n (y)	15.974	15.49 – 16.00	15.745 ± 0.255	C5Cn.1n: 6.342 ± 1.073	15.49 – 16.10	15.795 ± 0.305	C5Cn.1n: 6,359 ± 1.090
C5Cn.1n (o)	16.268	-5.80 – 0.00	-2.900 ± 2.900		-5.80 – 0.00	-2.900 ± 2.900	

Bioevent	Lower La Vedova Beach section						DSDP Site 372	
	hypothesis b_ Turco et al. 2011		hypothesis b_ This paper		Δ	(sub)chron	(Abdul Aziz et al. 2008, Di Stefano et al. 2008)	
	Mean strat. position (m)	Magnetostrat. Age (Ma)	Mean strat. position (m)	Magnetostrat. Age (Ma)	Age (Ma)		(sub)chron	Age (Ma)
G. dehiscens IB	54.970 ± 0.130	**15.072** ± 0.002	61.760 ± 0.130	**15.072** ± 0.002	0.000	C5Bn.2n	C5Bn.2n	-
P. gl. glomerosa FO	52.925 ± 0.085	**15.106** ± 0.001	59.715 ± 0.085	**15.105** ± 0.001	0.000	C5Bn.2n	C5Bn.2n	15.102
P. glomerosa curva FO	46.685 ± 0.135	**15.231** ± 0.003	53.475 ± 0.135	**15.218** ± 0.002	-0.013	C5Br	-	-
P. siakensis A_aE	46.065 ± 0.105	**15.246** ± 0.003	52.805 ± 0.055	**15.232** ± 0.001	-0.014	C5Br	C5Br	15.435
S. heteromorphus PE	45.430 ± 0.110	**15.261** ± 0.003	52.220 ± 0.110	**15.244** ± 0.002	-0.018	C5Br	C5Br	15.527
H. waltrans FRO	44.395 ± 0.115	**15.286** ± 0.003	51.185 ± 0.115	**15.264** ± 0.002	-0.022	C5Br	C5Br	15.476
P. siakensis A_aB	41.255 ± 0.095	**15.361** ± 0.002	48.045 ± 0.095	**15.327** ± 0.002	-0.034	C5Br	-	-
H. ampliaperta Ia_2E	36.220 ± 0.090	**15.482** ± 0.002	43.010 ± 0.090	**15.428** ± 0.001	-0.054	C5Br	-	-
H. ampliaperta AS	- -	- -	- -	- -	-	-	C5Br	15.899
H. ampliaperta Ia_2B	33.305 ± 0.105	**15.552** ± 0.003	40.095 ± 0.105	**15.487** ± 0.002	-0.066	C5Br	-	-
S. heteromorphus PB	29.480 ± 0.100	**15.644** ± 0.002	36.270 ± 0.100	**15.563** ± 0.002	-0.081	C5Br	C5Br	15.949
P. bella LCO	12.205 ± 0.095	**16.030** ± 0.001	12.205 ± 0.095	**16.030** ± 0.002	0.001	C5Cn.1n	-	-
H. ampliaperta LCO	10.490 ± 0.110	**16.057** ± 0.002	10.490 ± 0.110	**16.057** ± 0.002	0.001	C5Cn.1n	-	-
G. sicanus (3ap.) FO?	2.895 ± 0.185	**16.177** ± 0.003	2.895 ± 0.185	**16.177** ± 0.003	0.000	C5Cn.1n	-	-

the intervals between Megabeds II and III, VI and VII and X and XI, which are only weakly expressed (Figs. 2 and 4).

4.3 Planktonic foraminiferal proxies

The distribution pattern of *Globigerinoides trilobus* gr. and *Globigerinoides sicanus*/*Praeorbulina* gr. shows a rather consistent relationship with lithology (Fig. 4). These taxa show abundance fluctuations, which follow the megabed/marl interval alternation rather well. In particular, *G. trilobus* gr. is more abundant in the marl intervals between the megabeds (more evident in the lower part of the section) than in the megabeds. Superimposed on this large scale pattern, *G. trilobus* gr. often reveals abundance peaks in (or very close to) the greenish gray layers, which occur in clusters mainly in the marl intervals, whereas it is less abundant in the olive gray intervals. This relationship with sediment color is confirmed by the results of the Student t-Test analysis, which show higher abundances of *G. trilobus* gr. and *G. sicanus*/*Praeorbulina* gr. in the greenish gray layers (Table 2).

4.4 Geophysical proxy (MS)

Magnetic susceptibility (MS) is a sensitive indicator of changes in the marine sedimentary iron concentrations (e.g., Hay 1996, 1998, Ellwood et al. 2000) and hence of variability in terrigenous content, since iron is mainly supplied from land (Poulton and Raiswell 2002). MS record is shown in Figure 5, together with its 5 point moving average (pma) to reduce the effect of the noise and high-frequency variations and enhance main trends in the signal. The MS record tracks the megabed/marl interval alternation throughout the section, showing higher values in the marl intervals and lower values in the megabeds (Fig. 5). This pattern is more evident in the lower 40 m of the section, where the amplitude variation of the MS values between megabeds and marl intervals is more pronounced.

4.5 Geochemical proxies (XRF elemental record)

Here, we only present those elements or elemental ratios that are important for the tuning of the Lower La Vedova Beach section and the understanding of the cycles: Al, $CaCO_3$, Ca/Al, Si/Al, Rb/Sr, Rb/Al and Ti/Al. These records are shown in Figure 5, together with their 5 pma, and the results of the Independent Student t Test are presented in Table 2. The three extracted components of PCA respectively explain 25.51, 14.97 and 13.49 % of the total variance of the data set. Evaluation of the score plots showed that they are less indicative of the lithological alternation (i.e. megabeds) than the geochemical proxies selected above. For this reason, we decided to use the individual elemental records, but the component matrix and the score plots of the three extracted components are shown in Supplementary material B.

Al is considered as an useful indicator of the terrestrial fraction since it mainly resides in clays (e.g., Nijenhuis et al. 1996, Schenau et al. 1999). Al reveals distinct variations at the scale of megabed/marl inter-

Table 2 Average values in olive gray and in greenish gray layers and the *t* values resulting from an independent Student t Test performed on selected planktonic foraminiferal taxa and elemental ratios. The difference of the means of a proxy with respect to the two types of sediment color is statistically significant when $t_{(0.975)}$ value is > 1.96 for n = 239 samples (planktonic foraminifera) and n = 566 samples (elemental ratios).

Independent Student t Test			
	olive gray	greenish gray	$t_{(0.975)}$ value
Globigerinoides trilobus gr.	19.0302	30.5636	3.8476
Globigerinoides sicanus/*Praeorbulina* gr.	1.9064	4.8687	4.5096
Ca/Al	12.6132	14.3637	3.8996
Ti/Al	0.0476	0.0455	−2.2483
Zr/Al	0.0014	0.0012	−4.5502
V/Al	*0.0067*	*0.0060*	*−1.5367*
Ba/Al	*0.0219*	*0.0221*	*0.2436*
Rb/Al	0.0007	0.0006	−8.3759
Rb/Sr	*0.0175*	*0.0176*	*0.3573*

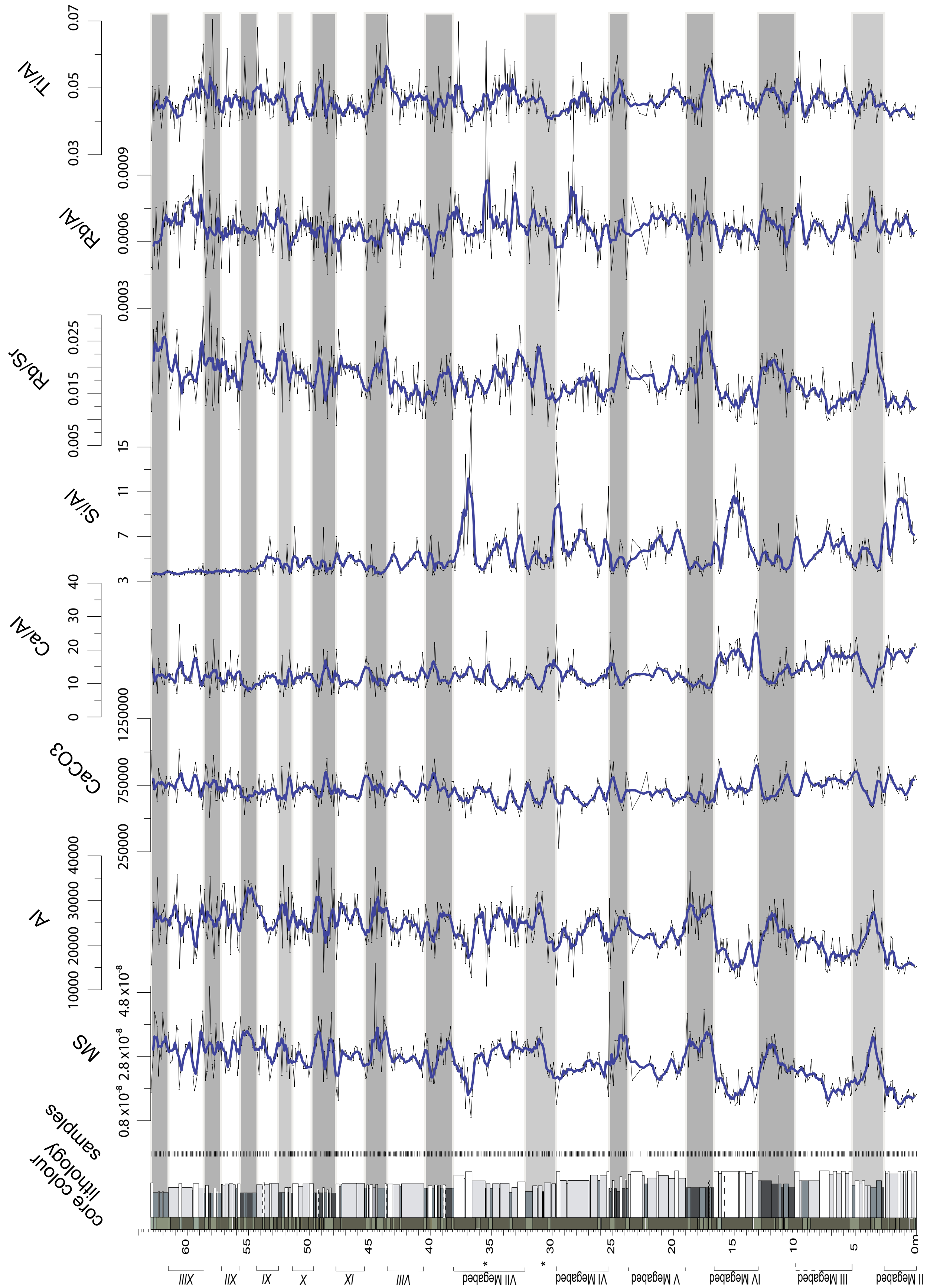

Fig. 5. The MS and the most relevant elemental (Al, $CaCO_3$, CA/Al, Rb/Sr, Si/Al, Rb/Al and Ti/Al) records and their 5 pma curves (blue lines) of the Lower La Vedova Beach section.

val alternation with higher values in the marl intervals; these are more evident in the true megabed interval in the lower part of the section. The amplitude variation of Al content between megabeds and marl intervals shows an upward decreasing trend similarly to MS. In addition, more prominent smaller-scale variations are observed in the upper half of the section.

The $CaCO_3$ record shows less distinct variations associated with the megabeds, but the marl intervals in between the megabeds are often marked by regular high-amplitude variations on a smaller-scale. Ca/Al reflects the relative carbonate content with respect to the input of clay assuming that most of Ca is derived from calcium carbonate (e. g., Mourik et al. 2010). The Ca/Al record shows large-scale variations with maxima associated with the megabeds in the lower 20 meters of the section. Upwards, the record continues to show variations linked with the thinner megabeds, but becomes dominated by more regular smaller-scale variations. Small-scale maxima of Ca/Al are statistically related to greenish gray layers (often limestones), as it is shown by Student t Test analysis (Table 2).

The Si/Al record shows strong variations related to the true megabeds in the lower 40 m of the section with distinct maxima associated with the megabeds. Similar variations, but with a much smaller amplitude, can be recognized up to Megabed XI above which the signal diminishes. Superimposed on this large-scale variability, the record shows small-scale variations, which are related to sediment color, having lower values in the greenish gray layers and higher values in the olive gray layers (Table 2).

Rb/Sr is considered as an indicator of chemical weathering intensity because Rb mainly occurs in

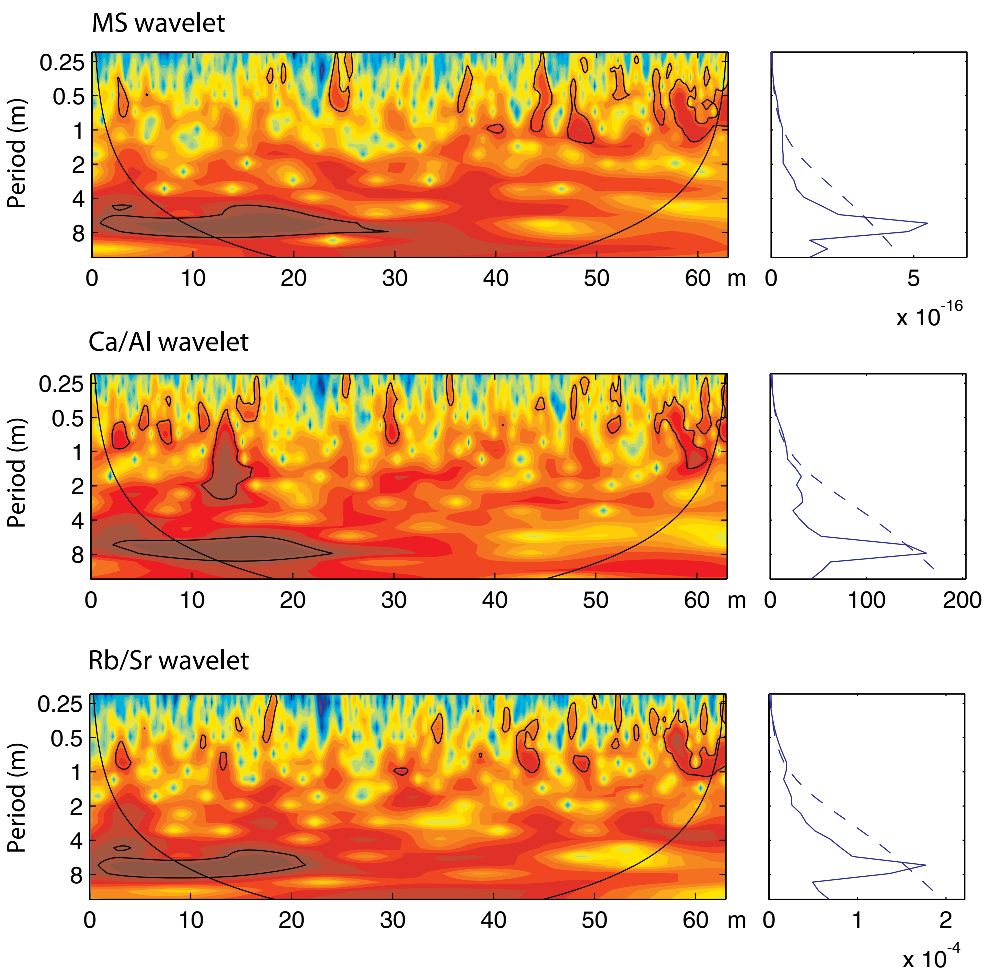

Fig. 6. Wavelet spectra of the MS, CA/Al and Rb/Sr records of the Lower La Vedova Beach section in the depth domain. Wavelet analysis was carried out using the Torrence and Compo (Torrence and Compo, 1998) method implemented in MATLAB. The autocorrelation coefficient of individual datasets and a Morlet wavelet was used.

K-bearing minerals, which are relatively resistant to weathering, and Sr remains in Ca-bearing minerals, which are sensitive to weathering (e.g., Chen et al. 1999). Rb/Sr shows clear variations related to the megabeds throughout the entire section with maxima in marl intervals. Regular variations on a smaller-scale are evident in the middle and upper part of the section (i.e., from 30 m up to the top).

The Rb/Al and Ti/Al records, the latter considered as an indicator of the aeolian terrestrial fraction and then the wind-borne terrestrial input (e.g., Nijenhuis et al. 1996), do not clearly track the megabed/marl interval alternations. On the contrary, they show regular small-scale variations that are thicker in the lower 20 m and become thinner in the upper part of the section. Small-scale variations seem to be related to sediment color, showing lower values in the greenish gray layers (Table 2).

4.6 Time series analysis

MS, Ca/Al and Rb/Sr proved to be the most suitable records for time series analysis. All wavelet spectra reveal the signature of a prominent ~7 m cycle in the lower 40 m of the section, which corresponds to Megabeds II–VII (Fig. 6). Upwards, a much less distinct 3–3.5 m cycle can be recognized in the Ca/Al wavelet spectra (Fig. 6), which may reflect the thinner megabeds described from this part of the section. In addition, enhanced power maxima associated with a 0.5–1.0 m cyclicity are recurrently observed between 40 and 63 m (Fig. 6).

The results of the wavelet analysis are confirmed by the outcome of the Blackman-Tukey spectral analysis; the latter was run separately for the 0–40 and 40–63 m intervals to avoid distortion caused by inferred changes in sedimentation rate suggested by the upward decrease in the thickness of the megabeds, as confirmed by the outcome of the wavelet analysis. The spectra of the two intervals reveal dominant peaks of ~7 and 3–3.5 m, respectively (Fig. 7). These cycles correspond to the alternation of megabeds and marl intervals identified in the section and show a similar decrease in thickness. The bandpass filtered ~7 m cycle in the lower part of the section agrees well with the megabeds. The same holds for the filtered 3–3.5 m cycles in Rb/Sr in the upper part of the section. However, in this part, the filtered MS and Ca/Al components suggest that one or two extra cycles are present in the interval between 40 and 50 m. Spectra in addition reveal peaks at higher frequencies that correspond to cycles with a thickness of ~1.5 and ~0.7 m in the lower and upper part of the section, respectively (Fig. 7). Bandpass filtering of these cycles, applied to Ca/Al, $CaCO_3$ and Rb/Al records, reveals amplitude variations often higher in the marl intervals in between the megabeds (Fig. 8).

5. Tuning and astronomical time scale

5.1 Tuning to eccentricity

The calibration of the magnetostratigraphy to the polarity time scale of the ATNTS2012 (Hilgen et al. 2012) (Fig. 4) suggests that the megabed scale alternations are related to the ~100-kyr eccentricity cycle with 10.5 alternations in 1.1 myr, between 16.268 (C5Cn.1n(o) at −2.90 m, Turco et al. 2011a) and 15.160 Ma (C5Bn.2n(o) at 56.385 m, this paper). The same holds for the associated 7 and 3–3.5 m cycles detected by time series analysis of the proxy records (Fig. 7). However, to establish a tuning, the phase relation between the megabed/marl interval alternations and eccentricity should also be known. In the Lower La Vedova Beach section, the records, which best show variability on the megabed scale throughout the succession, are those of the *G. trilobus* gr., MS and Rb/Sr (Fig. 9). Following the previously established phase relation between these proxies and precession/eccentricity cycles (e.g., Zinsheng et al. 2001, Sprovieri et al. 2002) maxima in the *G. trilobus* gr. (albeit less clear in the upper part of the section), MS and Rb/Sr suggest that the marl intervals in between the megabeds correspond to eccentricity maxima. Consequently, mega-

Fig. 7. A) Blackman-Tukey spectra of the MS, Ca/Al and Rb/Sr records for the 0–40 m interval in the Lower La Vedova Beach section in the depth domain and results of bandpass filtering of the prominent ~7 m cyclicity; B) Blackman-Tukey spectra of the MS, Ca/Al and Rb/Sr records for the 40–63 m interval in the Lower La Vedova Beach section in the depth domain and results of bandpass filtering of the prominent ~3–3.5 m cyclicity at frequencies of 0.30 ± 0.20, 0.36 ± 0.084, 0.35 ± 0.15 and 0.28 ± 0.12 cycle/m, respectively. The Analyseries program of Paillard et al. (1996) and 80 % confidence level were used. The 80 % confidence level interval is indicated by the lower and upper spectra (red and green lines, respectively).

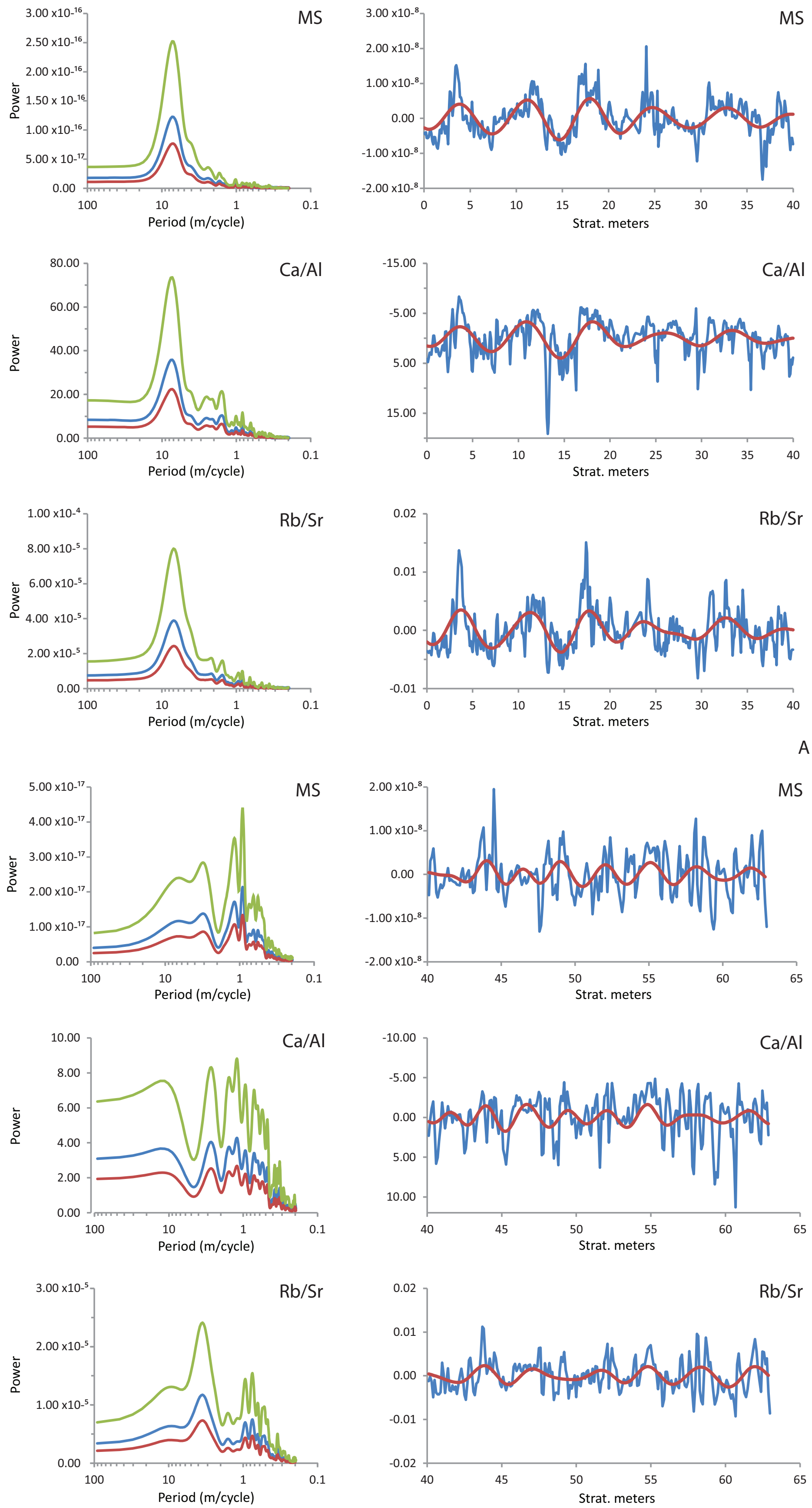
MS
Power
3.00 x10-16
2.50 x10-16
2.00 x10-16
1.50 x 10-16
1.00 x10-16
5.00 x 10-17
0.00
100
10
1
0.1
Period (m/cycle)
MS
3.00 x10-8
2.00 x10-8
1.00 x10-8
0.00
-1.00 x10-8
-2.00 x10-8
0
5
10
15
20
25
30
35
40
Strat. meters
Ca/Al
Power
80.00
60.00
40.00
20.00
0.00
Period (m/cycle)
Ca/Al
-15.00
-5.00
5.00
15.00
Strat. meters
Rb/Sr
Power
1.00 x10-4
8.00 x10-5
6.00 x10-5
4.00 x10-5
2.00 x10-5
0.00
Period (m/cycle)
Rb/Sr
0.02
0.01
0.00
-0.01
Strat. meters
A
MS
Power
5.00 x10-17
4.00 x10-17
3.00 x10-17
2.00 x10-17
1.00 x10-17
0.00
Period (m/cycle)
MS
2.00 x10-8
1.00 x10-8
0.00
-1.00 x10-8
-2.00 x10-8
40
45
50
55
60
65
Strat. meters
Ca/Al
Power
10.00
8.00
6.00
4.00
2.00
0.00
Period (m/cycle)
Ca/Al
-10.00
-5.00
0.00
5.00
10.00
Strat. meters
Rb/Sr
Power
3.00 x10-5
2.00 x10-5
1.00 x10-5
0.00
Period (m/cycle)
Rb/Sr
0.02
0.01
0.00
-0.01
-0.02
Strat. meters

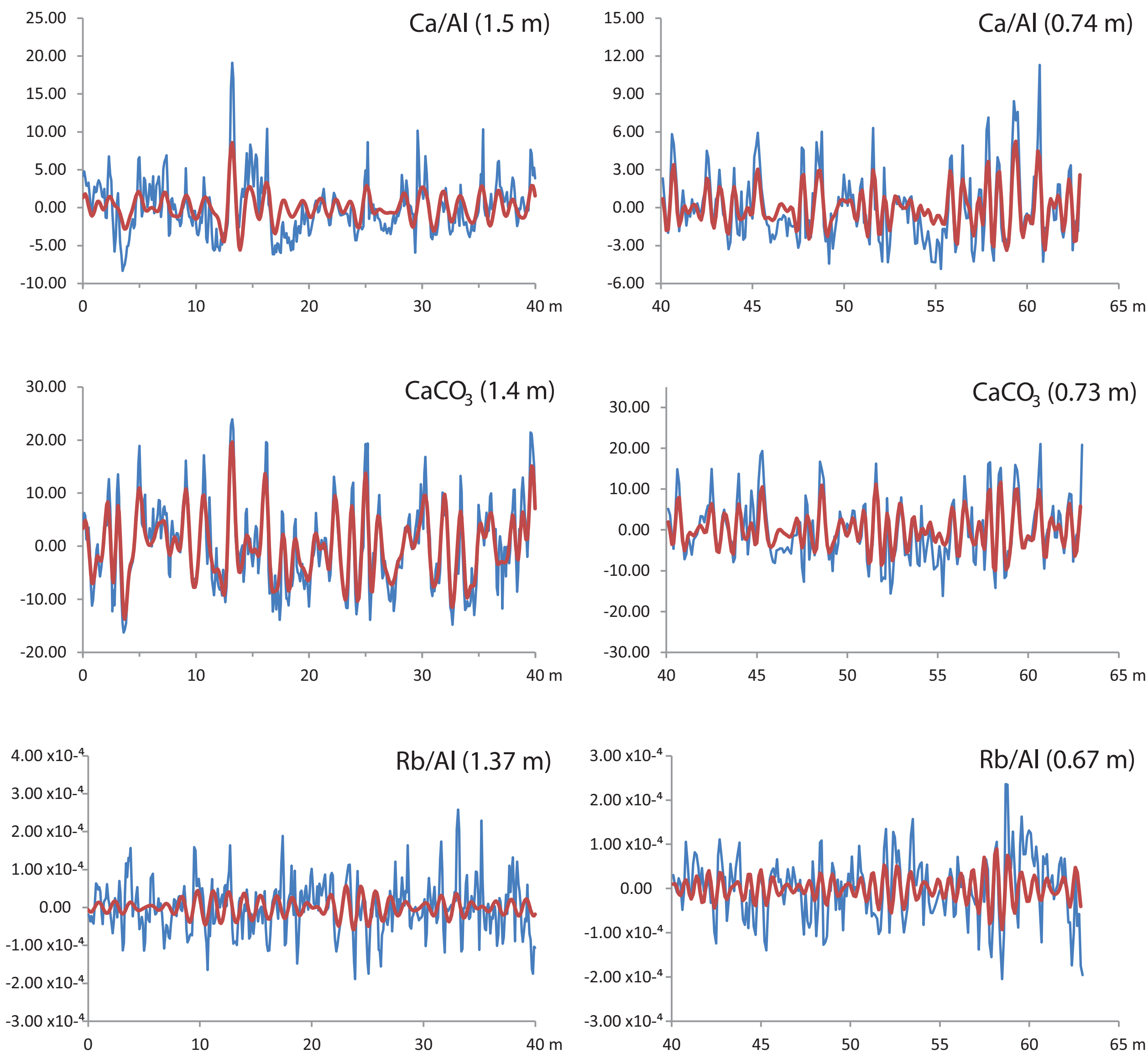

Fig. 8. Bandpass filtering of the higher frequency spectral peaks at frequencies of 0.65 ± 0.35 (Ca/Al), 0.70 ± 0.65 ($CaCO_3$) and 0.73 ± 0.14 (Rb/Al) cycle/m, corresponding to ~ 1.5 m in the 0–40 m interval, and at frequencies of 1.35 ± 0.85 (Ca/Al), 1.37 ± 0.85 ($CaCO_3$) and 1.50 ± 0.32 (Rb/Al) cycle/m, corresponding to ~ 0.7 m in the 40–63 m interval.

beds correspond to eccentricity minima. A similar phase relation is also suggested by the clusters of greenish gray layers and the preferentially higher amplitudes of the filtered higher frequency proxy cycles occurring in the marl intervals (Fig. 8). In view of the ratio thickness of the cyclicity, these high frequency cycles should correspond to precession and the observed amplitude variations to the amplitude modulation of precession by eccentricity.

For the tuning to eccentricity, we preferred to start from the megabed/marl interval alternations rather than to use the bandpass filtered components. The reason for this is that the outcome of the bandpass filtering is complicated by the reduction in thickness of the megabed/marl interval alternations in the section, supposedly reflecting a lowering of the sedimentation rate. This reduction in thickness of the megabed scale cycles does not occur abruptly, but rather gradually between 40 and 50 m, and may explain the one or two extra cycles that are observed in the bandpass filtered components in MS and Ca/Al in this interval.

The tuning can proceed from the top of the section downward, following the previously established tuning of the younger Upper La Vedova Beach section

(Hüsing et al. 2010) to which it is stratigraphically connected. The top of the Lower La Vedova Beach section thus coincides with the base of the distinctive interval with thinly bedded limestones that marks the 405-kyr eccentricity minimum around 15.0 Ma (Hüsing et al. 2010). Megabeds XIII to II in our section are tuned to successively older ~100-kyr eccentricity minima, following this 405-kyr minimum (Fig. 9). The resulting tuning is consistent with the weakly developed marl intervals between Megabeds X and XI, VI and VII, II and III, which mark the low amplitude ~100-kyr maxima in the 405-kyr minima at 15.4 Ma, 15.8 and 16.2 Ma, respectively. The 3 distinct marl intervals between Megabed XI and the top of the section, Megabeds VII and X, Megabeds III and VI correspond to the three prominent ~100-kyr maxima which denote the 405-kyr maxima around 15.2 Ma, 15.6 Ma and 16.00 Ma, respectively. According to this tuning, the thick Megabeds III and VII coincide with marked ~100-kyr minima at 16.13 and 15.75 Ma,

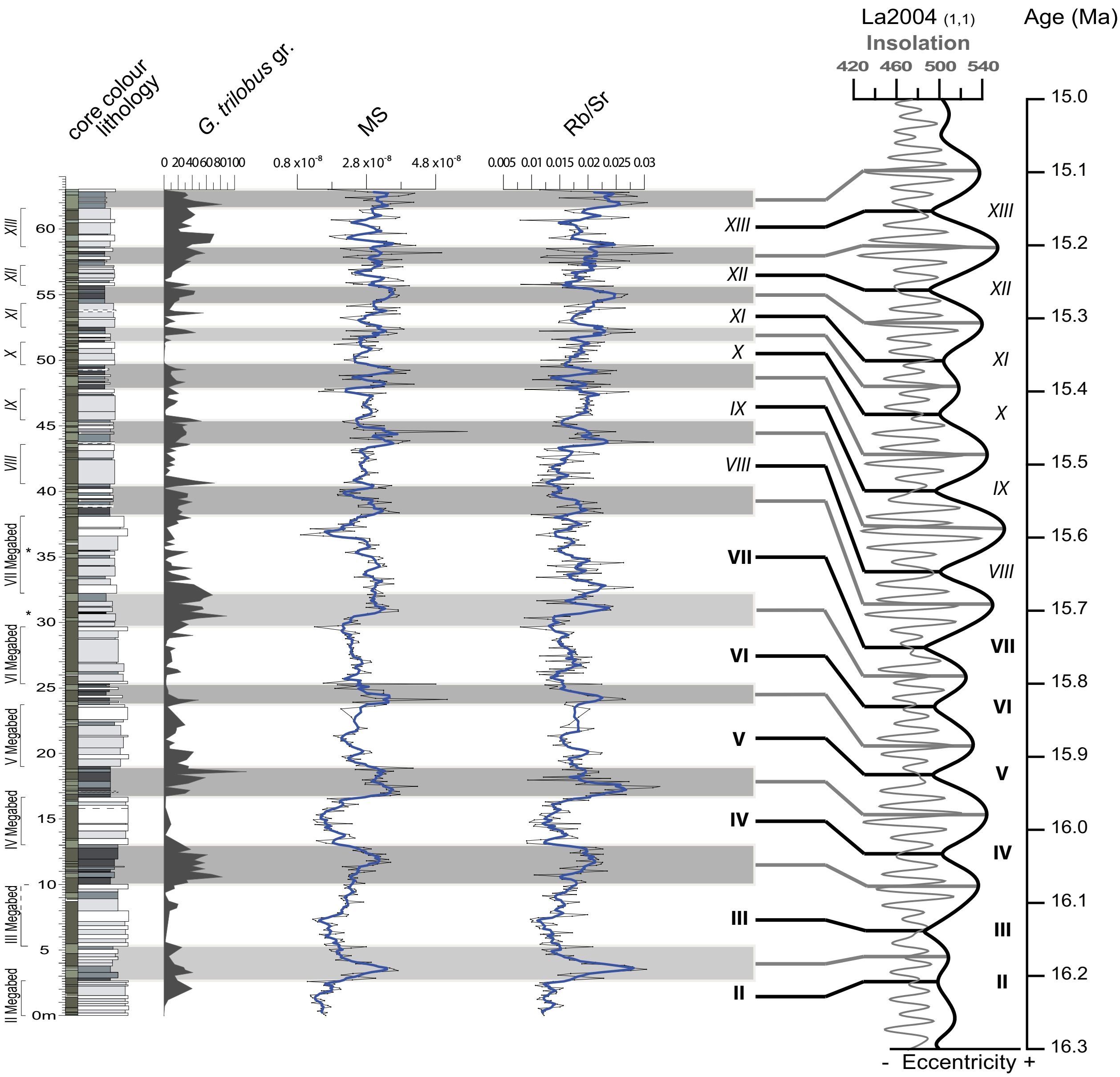

Fig. 9. Tuning of the Lower La Vedova Beach section to the Laskar $2004_{(1,1)}$ eccentricity target curve. The middle points of megabeds and the intervening marl intervals have been correlated to minima and maxima of 100 kyr eccentricity, respectively. The phase relation is inferred from *G. trilobus* gr., MS and Rb/Sr records. The 5 pma of MS and Rb/Sr records (blue lines) are plotted on top of the raw data (black lines).

while the thinner Megabeds II and IV correspond to weak ~100-kyr minima. Further constraints come from the tuning of the downward extension of our section near Ancona (unpublished data). The elemental proxy records in this section reveal a marked increase in amplitude of the signal associated with the precession related cyclicity below the megabeds. This increase logically reflects the 405-kyr eccentricity maximum around 16.4 Ma marked by two distinct ~100-kyr maxima (unpublished data). Note, however, that *G. trilobus* gr., MS and Rb/Sr maxima do not perfectly fit with the pattern of eccentricity maxima (e.g., *G. trilobus* gr. pronounced maximum in the marl interval between Megabeds VI and VII, which supposedly corresponds to a weak 100 kyr eccentricity maximum) (Fig. 9).

The tuning to eccentricity was used to establish a first order astronomical age model with two tie-points per 100-kyr cycle. These tie-points were visually selected as the midpoints of the calcareous and marl intervals of the cycles and tuned to the correlative minimum and maximum eccentricity, respectively. This age model was used to establish eccentricity tuned time series for the proxy records. Not surprisingly, spectral

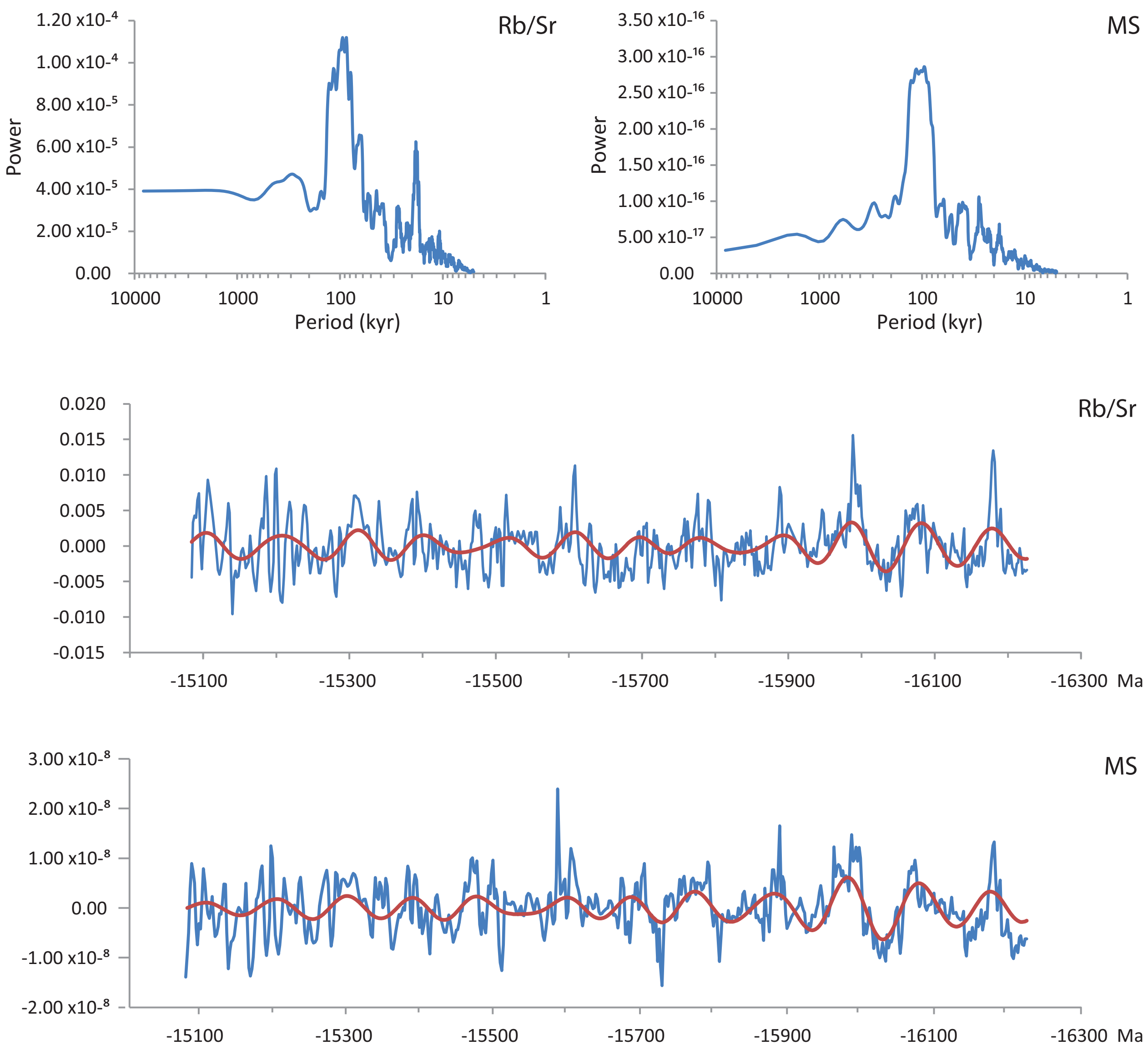

Fig. 10. MTM spectra of the eccentricity tuned Rb/Sr and MS time series and comparison of the extracted ~100-kyr cycle with eccentricity.

analyses of these time series revealed the presence of a ~100-kyr eccentricity-related cycle as the proxy records have been tuned to eccentricity (Fig. 9). This eccentricity related signal was extracted by means of bandpass filtering and is compared with eccentricity in Figure 10. However, spectral analysis also detected precession-related variability (Fig. 11). Bandpass filtering was applied to extract this signal from the Rb/Sr and Rb/Al time series, which show this scale of cyclicity most clearly (Figure 11). All filtered components are shown as overlay on the proxy records for direct comparison with the time series (Figs. 10 and 11).

5.2 Tuning to precession and insolation

The final age model is generated by the tuning of the high frequency cyclicity to precession and 65° Nlat summer insolation. The latter is widely used as target curve in the Mediterranean for reasons outlined in Lourens et al. (1996) and provides a good fit with the cycle patterns. However, a recent modeling study (Bosmans et al. 2015) suggests that alternative target curves can better be used, as the forcing of both the precession and obliquity signal likely comes from low-latitudes. Nevertheless, the insolation patterns remain essentially

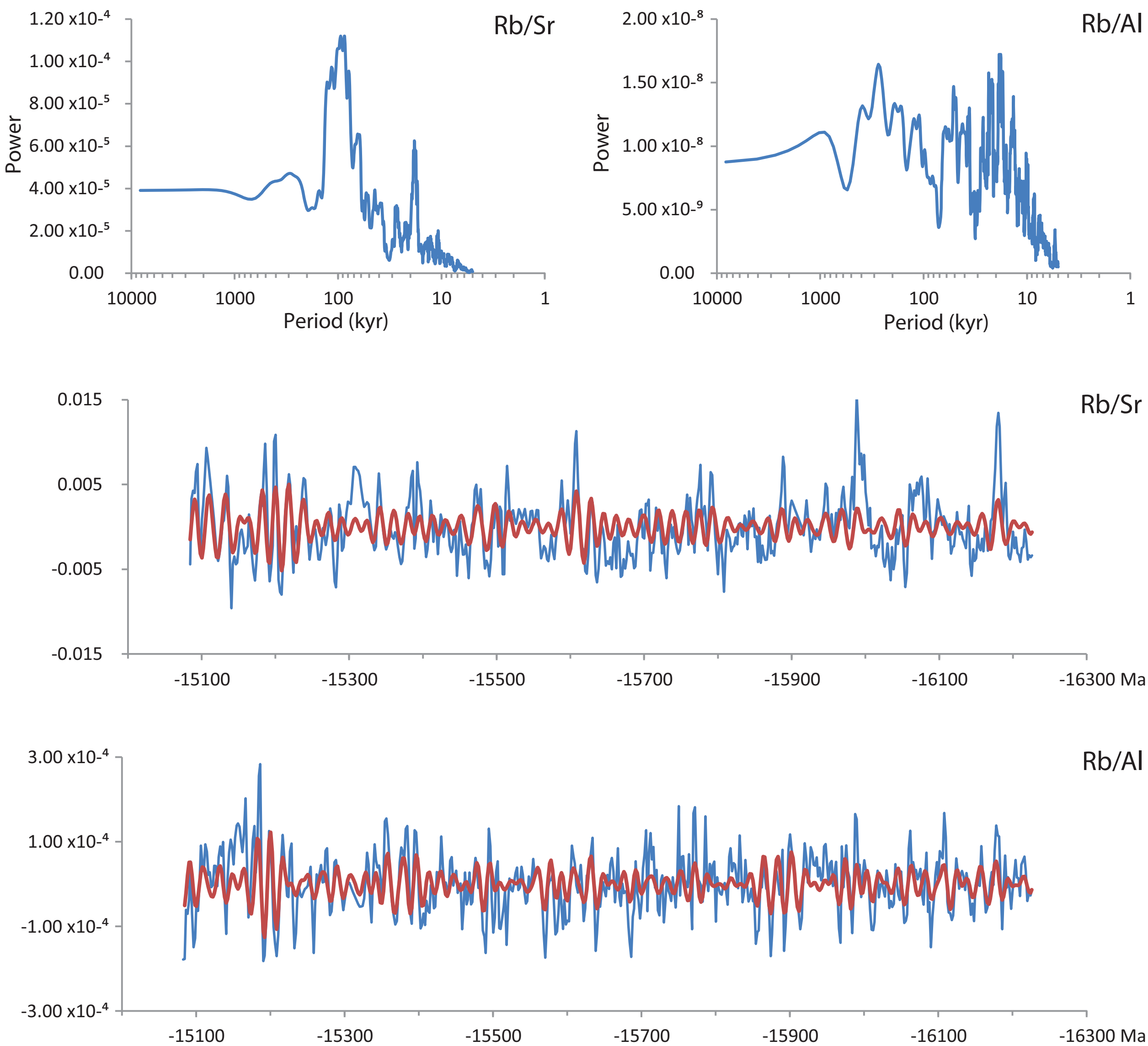

Fig. 11. MTM spectra of the eccentricity tuned Rb/Sr and Rb/Al time series and bandpass filtered precession-related components shown as overlay on these time series.

the same and, for this reason, we stick here to the classical 65° Nlat summer insolation curve. For the tuning at the precession scale, again the phase relation with the target curve(s) has to be known. However, the issue of the phase relation of the cycles with precession and insolation has proven to be particularly challenging because the structure of the basic cycle in the section is not clearly developed and the phase relation between proxies and astronomical cycle may have changed over time. Following the Mi 3b shift to heavy values in $\delta^{18}O$ at 13.8–13.9 Ma, which marks the end of the Middle Miocene Climate Transition and the occurrence of the first sapropelitic layers in basic precession-controlled cycles typical of the Mediterranean late Neogene (Mourik et al. 2010), the phase relation with precession and insolation is relatively straightforward. Sapropels, associated with maxima in redox-sensitive elements (such as V) and productivity indicator Ba/Al and with minima in aeolian terrestrial fraction indicators, such as Ti/Al, Zr/Al, Rb/Al, and planktonic foraminifera $\delta^{18}O$ and $\delta^{13}C$ (e.g., De Visser et al. 1989, Van Os et al. 1994, Nijenhuis et al. 1996, Schenau et al. 1999, Wehausen and Brumsack 2000, Calvert and Fontugne 2001, Mourik et al. 2010), correspond to precession minima and obliquity maxima, and hence to (boreal) summer insolation maxima. This phase relation remains remarkably constant up to the most recent sediments deposited in the Mediterranean, although the youngest sapropels of late Quaternary may reveal a time lag of up to ~3 kyr relative to the astronomical forcing due to the influence of the ice ages and cold climate phases, such as the Younger Dryas, that occur superimposed on deglaciations (Ziegler et al. 2010), or to magnitude of meltwater pulses in combination with sea-level rise (Grant et al. 2016). Sapropels are further often associated with maxima in the planktonic foraminifera *Globigerinoides* spp. (Sprovieri 1992, Nijenhuis et al. 1996, Schenau et al. 1999, Sprovieri et al. 2006). On the contrary, the phase relation between limestone beds (associated with Ca-maxima) and precession/insolation is not constant. In the Pliocene Trubi Formation limestone beds correspond to precession maxima/insolation minima (Hilgen 1991), whereas in the middle Miocene Monte dei Corvi beach section limestone beds, in which sapropels tend to develop, correspond to precession minima/insolation maxima (Hilgen et al. 2003).

Prior to the Mi 3b oxygen isotope increase, the phase relation between the proxies changed, although not abruptly. In the La Vedova High Cliff section between 14.2 and 13.8 Ma Ti/Al minima mostly correspond to V/Al minima and Ca/Al maxima, and to $\delta^{13}C$ and to a lesser extent $\delta^{18}O$ maxima (Mourik et al. 2010). This relation between proxies seems to be similar to that observed in the older Upper La Vedova Beach section (Hüsing 2008, Hüsing et al. 2010) and in its downward extension (this paper). The question that remains is which phase relations with precession and insolation remain constant and which phase relations become reversed. In the Upper La Vedova Beach section between 15.29 and 14.17 Ma, limestone beds (Ca-maxima) are often associated with minima in MS and maxima in Ba/Al and V/Al, whereas their relationship with Ti/Al and Zr/Al is not consistent throughout the entire section (Hüsing 2008, Hüsing et al. 2010). Limestone beds were initially tuned to precession minima/summer insolation maxima, on the basis of the associated V/Al and Ba/Al maxima (Hüsing 2008, PhD-thesis); this phase relation was based on the assumption that the sedimentary expression of sapropels is lacking, but that the associated reducing conditions are still expressed as V/Al maxima. However, in the paper that was subsequently published (Hüsing et al. 2010), the same limestone beds were tuned to precession maxima/summer insolation minima assuming an opposite phase relation following suggestions by the referees on the basis of the heavier values of bulk $\delta^{18}O$ and $\delta^{13}C$ isotopes observed in the limestone beds (Mader et al. 2004).

In the Lower La Vedova Beach section (this paper), the build-up of the basic cycles is not clearly expressed even in the marl intervals, between the megabeds, corresponding to 100 kyr eccentricity maxima. However, the core color record shows that the greenish gray layers are intercalated in the predominant olive gray sediments; these layers are composed of marls or marls associated with a limestone bed at the base or at the top. The clustering of these greenish gray layers in the marl intervals corresponding to 100 kyr eccentricity maxima, suggests that they are the expression of the precession scale cyclicity. This high frequency cyclicity is also portrayed by the proxy records as MS, Rb/Sr, Ti/Al, Rb/Al and Ca/Al (Fig. 12). In particular, minima in Ti/Al, Rb/Al, Rb/Sr and MS, and maxima in Ca/Al are generally found in the greenish gray layers. These layers are also associated with maxima in the *G. trilobus* gr. (Table 2). Assuming that the phase relation of the terrestrial fraction indicators and *Globigerinoides* with precession/insolation cycles remains constant, then minima in Ti/Al, Rb/Al, Rb/Sr and MS and associated maxima in Ca/Al correspond to precession minima/insolation maxima, of which the greenish gray layers are the lithological expression. Accordingly, we used this phase relation to tune the section to the Laskar $2004_{(1,1)}$ insolation target curve (Laskar et al. 2004) (Fig. 12). Starting point was the tuning of the megabed/marl interval alternations to eccentricity with the marl intervals corresponding to 100 kyr maxima and the megabeds to the 100 kyr minima (Fig. 9). First we tuned the precession scale cycles in marly intervals to high amplitude insolation cycles in the correlative 100-kyr eccentricity maximum. The tuning was then expanded by correlating precession scale cycles in the megabeds to low amplitude insolation cycles in the correlative 100 kyr eccentricity minimum (Fig. 12). The tie points used for the tuning to insolation curve are indicated by crosses and were selected considering the high frequency variability of all the proxies (Fig. 12).

However, in view of the uncertainties of the phase relation between Ca-maxima and precession/insolation cycles (e.g., Mader et al. 2004, Husing et al. 2010) we also prepared a tuning based on the opposite phase relation (Supplementary material C, Fig. C1).

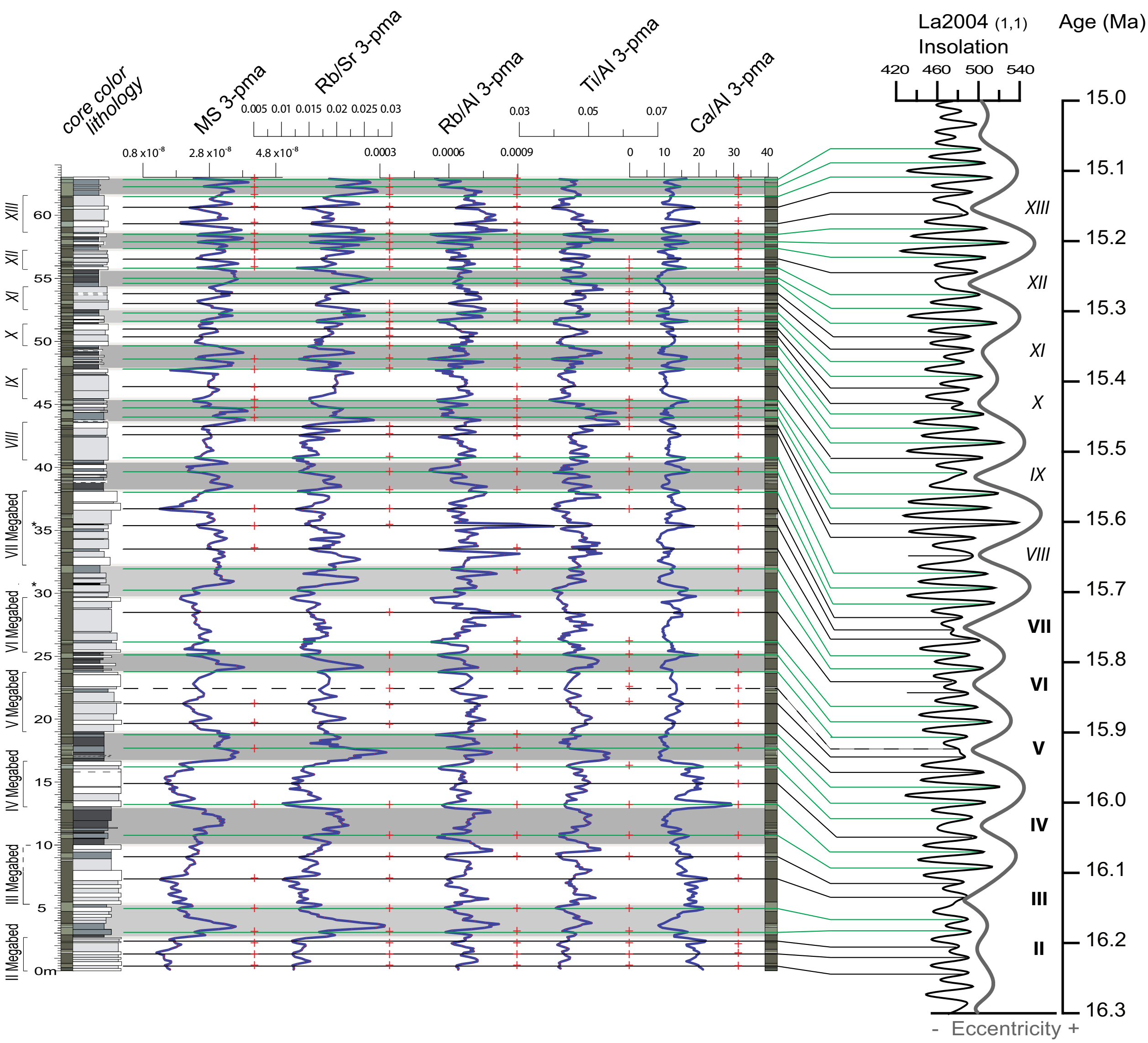

Fig. 12. Tuning of the MS, Rb/Sr, Rb/Al, Ti/Al and Ca/Al 3 pma records of the Lower La Vedova Beach section to the Laskar $2004_{(1,1)}$ 65N lat summer insolation. The tie-points used for the tuning are indicated by crosses.

Table 3 Astronomical ages of magnetic reversal boundaries and calcareous plankton events according to the tuning to eccentricity and insolation. It is also indicated the age difference of magnetic reversals between ATNTS2012 and the astronomical calibration to eccentricity at La Vedova (Δ1), between ATNTS2012 and the astronomical calibration to insolation at La Vedova (Δ2), and between the astronomical calibration to eccentricity and to insolation at La Vedova (Δ3). Astronomical calibration of calcareous plankton events is compared with the magnetostratigraphic age. It is indicated the age difference of the bioevents between magnetostratigraphic and astronomical calibration to eccentricity at La Vedova (Δ1), between magnetostratigraphic and astronomical calibration to insolation (Δ2) and between astronomical calibration to eccentricity and to insolation (Δ3). Astronomical ages are calculated by means of linear interpolation between the two nearest calibration points assuming constant sedimentation rates.

Magnetic reversal boundaries	Stratigraphic position (m)			ATNTS 2012 (Ma)	Astronomical calibration eccentricity (Ma)			Astronomical calibration insolation (Ma)			Δ 1(Ma)	Δ 2 (Ma)	Δ3 (Ma)
C5Bn.2n (o)	56.385	±	0.305	**15.160**	**15.264**	±	0.009	**15.251**	±	0.013	-0.104	-0.091	0.013
C5Cn.1n (y)	15.795	±	0.305	**15.974**	**16.017**	±	0.005	**16.030**	±	0.006	-0.043	-0.056	-0.012

Bioevents	Mean strat. position (m)			(sub)chron	Magnetostratigraphic calibration (Ma)			Astronomical calibration Eccentricity (Ma)			Astronomical calibration Insolation (Ma)			Δ 1 (Ma)	Δ 2 (Ma)	Δ3 (Ma)
G. dehiscens IB	61.760	±	0.130	C5Bn.2n	**15.072**	±	0.002	**15.113**	±	0.003	**15.101**	±	0.003	-0.041	-0.030	0.011
P. gl. glomerosa FO	59.715	±	0.085	C5Bn.2n	**15.105**	±	0.001	**15.163**	±	0.002	**15.153**	±	0.002	-0.057	-0.048	0.010
P. glomerosa curva FO	53.475	±	0.135	C5Br	**15.218**	±	0.002	**15.356**	±	0.004	**15.343**	±	0.004	-0.137	-0.125	0.013
P. siakensis A_aE	52.805	±	0.055	C5Br	**15.232**	±	0.001	**15.374**	±	0.001	**15.359**	±	0.001	-0.142	-0.128	0.014
S. heteromorphus PE	52.220	±	0.110	C5Br	**15.244**	±	0.002	**15.389**	±	0.003	**15.372**	±	0.004	-0.145	-0.128	0.017
H. waltrans FRO	51.185	±	0.115	C5Br	**15.264**	±	0.002	**15.414**	±	0.003	**15.403**	±	0.003	-0.150	-0.138	0.012
P. siakensis A_aB	48.045	±	0.095	C5Br	**15.327**	±	0.002	**15.502**	±	0.002	**15.480**	±	0.002	-0.175	-0.153	0.022
H. ampliaperta Ia_2E	43.010	±	0.090	C5Br	**15.428**	±	0.001	**15.625**	±	0.002	**15.608**	±	0.003	-0.197	-0.180	0.018
H. ampliaperta Ia_2B	40.095	±	0.105	C5Br	**15.487**	±	0.002	**15.680**	±	0.002	**15.687**	±	0.002	-0.193	-0.200	-0.007
S. heteromorphus PB	36.270	±	0.100	C5Br	**15.563**	±	0.002	**15.736**	±	0.001	**15.742**	±	0.001	-0.172	-0.178	-0.006
P. bella LCO	12.205	±	0.095	C5Cn.1n	**16.030**	±	0.002	**16.067**	±	0.001	**16.078**	±	0.001	-0.037	-0.048	-0.011
H. ampliaperta LCO	10.490	±	0.110	C5Cn.1n	**16.057**	±	0.002	**16.093**	±	0.002	**16.094**	±	0.001	-0.036	-0.036	-0.001
G. sicanus (3ap.) FO?	2.895	±	0.185	C5Cn.1n	**16.177**	±	0.003	**16.189**	±	0.002	**16.189**	±	0.005	-0.012	-0.012	0.000

6. Discussion

6.1 Magnetobiostratigraphy and astronomical calibration

The tuning results in astronomical ages for magnetic reversal boundaries and calcareous plankton events recorded in the Lower La Vedova Beach section. These events were calibrated starting from both the tuning to eccentricity and to insolation (Table 3). The ages for the C5Cn.1n/C5Br and C5Br/C5Bn.2n boundaries are older than the ages for the same boundaries in the most recent standard Geological Time Scale (ATNTS2012 of Hilgen et al. 2012), where they were calibrated by means of interpolation of seafloor spreading rates using anomaly profiles from the Pacific. In the Lower La Vedova Beach section the C5Cn.1n/C5Br boundary is dated 43/56 kyrs older than in ATNTS2012 at 16.017/16.030 Ma; the age difference between our calibration and ATNTS2012 is greater (104/91 kyrs) for the C5Br/C5Bn.2n boundary dated at 15.264/15.251 Ma (Table 3). This age discrepancy does not seem to be due to tuning problems, since the tuning of the Lower La Vedova Beach section is consistent with the tuning of the younger Upper La Vedova Beach section of Hüsing et al. (2010) and the succession below the megabed interval as exposed in sections near Ancona (unpublished data).

The astronomical ages for the calcareous plankton events (based on the tuning to eccentricity and to insolation) are presented in Table 3 and compared with the magnetostratigraphic ages according to the revised age model of Turco et al. (2011a) in this study. The astronomical ages are different with age discrepancies up to ~ 50 kyr for the bioevents recorded in the short normal polarity intervals (C5Cn.1n and C5Bn.2n) and up to 200 kyr for the bioevents associated with the long reversed interval (C5Br). The astronomical ages should be considered more reliable than the magnetostratigraphic ages for several reasons. In the first place, the tuning is likely correct on the eccentricity scale, based on the agreement between the cycle pattern and the eccentricity target curve. Secondly, the number of tie-points in the magnetostratigraphic age model is limited so that constant sedimentation rates had to be inferred over prolonged stratigraphic intervals, while the thinning of the megabeds suggests a reduction in sedimentation rate in the middle reversed part of the section.

The integrated magnetobiostratigraphy and tuning of the La Vedova section can be tested by comparison with the Moria section (Marche region, central Italy). The latter section has not been tuned and has a low resolution magnetostratigraphy, but single crystal $^{40}Ar/^{39}Ar$ dates for several ash-beds and a high-resolution calcareous plankton biostratigraphy are available (Deino et al. 1997, Di Stefano et al. 2008). The $^{40}Ar/^{39}Ar$ ages were calculated, using an age of 27.84 Ma for the Fish Canyon sanidine (FCs) dating standard, but have been recalculated relative to the astronomically calibrated FCs age of 28.201 Ma (Kuiper et al. 2008) for direct comparison with our astronomical tuning of La Vedova. The two youngest of the three ash-beds dated in the Moria section by Deino et al. (1997) are relevant for our study. They are intercalated in the Siliceous-Calcareous Member of the Schlier Formation, which corresponds to the interval of the Massive Member marked by the seven Megabeds at La Vedova. The top of both these stratigraphic intervals is closely approximated by the base of the *Sphenolithus heteromorphus* Paracme and falls within the second influx of *Globoturborotalita woodi*, indicating that this level is synchronous between the sections (Deino et al. 1997, Di Stefano et al. 2008, Turco et al. 2011a and this paper). However, it is not clear whether the base of these members is also synchronous in the two sections, due to lack of high-resolution biostratigraphic control in this interval.

The stratigraphic position of the youngest dated Moria ash-bed (76.8 m in the section of Deino et al. 1997 corresponding to the level of 28 m in the section of Di Stefano et al. 2008) is close to the top of the Siliceous-Calcareous member, just below the base of the *S. heteromorphus* Paracme and the second influx of *G. woodi* (Deino et al. 1997, Di Stefano et al. 2008, Turco et al. 2011a). This suggests that this ash-bed corresponds with that detected at La Vedova at 35 m (Fig. 4). Unfortunately, the age of the Moria ash-bed is complicated by a bimodal age distribution, but its recalculated age of 15.70 ± 0.16 Ma is nevertheless within error consistent with the estimated astronomical age of ~ 15.75 Ma at La Vedova (Fig. 9) and thus in agreement with our tuning. The other dated ash-bed of interest, located at 58.4 m in the Moria section of Deino et al. (1997), likely corresponds to one out of two ash-beds found at ~ 13 and 11 m in the same section by Di Stefano et al. (2008). Both ash-beds are intercalated well below the *Helicosphaera ampliaperta* LCO (Di Stefano et al. 2008). Downward extrapolation of the sedimentation rate, calculated with the help of the astronomical ages for the base of the first influx of *G. woodi* gr. (16.014 Ma) and the *H. ampliaperta* LCO (16.094 Ma), results in respective ages of

~ 16.25 Ma and 16.33 Ma for these two ash layers at Moria. These ages are within error consistent with the recalculated single crystal $^{40}Ar/^{39}Ar$ sanidine age of 16.39 ± 0.16 Ma. These ash-beds have not been detected in the Lower La Vedova Beach section, but should be located below the base of the section again in agreement with our tuning. The detailed comparison reveals that our astronomical tuning of the Lower La Vedova Beach section is in agreement with the independent radio-isotopic age constraints from the Moria section. It further shows that the published magnetostratigraphy of the La Moria section and its calibration to the polarity time scale are likely flawed.

6.2 Phase relations

The problem of the phase relation with precession and insolation is fundamental but complex. Evidently, the relation between the proxies changes across the Mi 3b event and, thus, the associated glacio-eustatic sea-level lowering and/or climate changes were likely responsible for this change. If we assume that prior to Mi 3b event the phase relation between Ca/Al, V/Al, Ti/Al and Zr/Al with precession remained constant then the phase relation with the oxygen and carbon bulk isotopes became opposite. In that case, Ca/Al and V/Al maxima and Ti/Al and Zr/Al minima correspond to precession minima and summer insolation maxima, just as is the case for the interval younger than the Mi 3b. The V/Al maxima may point to reducing conditions, but sapropels did not develop. Note, however, that the distinct quadripartite structure of the precession related cycles above the Mi 3b event with the development of sapropels in the limestone beds complicates the relation between Ca/Al maxima and precession minima. In the presently studied section, the greenish gray marl/limestones show the same phase relation, being characterized by Ca/Al maxima and Ti/Al and Zr/Al minima, although V/Al does not show an univocal relationship with these layers (Table 2). The Ti/Al and Zr/Al minima can be explained by an enhanced fluvial signal, while the maxima in the opposite phase of the cycle point to a relatively larger input of eolian material. Sapropels only develop after the Mi 3b, suggesting an intensification of the African monsoon or, alternatively, that this part of the Mediterranean became more enclosed, possibly as a consequence of the sea-level lowering associated with the Mi 3b, and, therefore, more sensitive to monsoonal or Atlantic induced climate variability. This may also explain why the isotope shifts to lighter values started to be recorded in the sapropels and/or the associated limestone beds only from the Mi 3b onwards. Before the Mi 3b the $\delta^{18}O$ shifts to heavier values in the limestone beds may be explained by the fact that they do not record the summer signal with the stronger heating and enhanced outflow of fluvial run-off, but instead the colder winters which are also associated with precession minima.

According to this scenario, the limestone, or Ca/Al maxima, correspond to the basic couplet/doublet limestone-marl cycle as depicted in Hilgen et al. (2003, their Fig. 2) with sapropels starting to be intercalated in the limestone beds above the Mi 3b during eccentricity maxima when precession amplitudes are enhanced, resulting in the characteristic quadruplet structure of the cycles in the upper part of the La Vedova High Cliff and lower part of the Monte dei Corvi sections. According to the alternative scenario, the phase relation between limestone beds, or Ca/Al maxima, would become opposite across the Mi 3b. The limestone beds and intercalated sapropels correspond to precession minima from ~ 13.8 Ma onwards, while they correspond to precession maxima in older intervals. For the moment, we consider the first option with the limestones beds and associated maxima in Ca/Al and *G. trilobus* gr. and minima in Ti/Al and Zr/Al corresponding to precession minima more likely, as that implies less drastic changes in the underlying climate changes.

The uncertainty in the phase relation between sedimentary cycles and precession (and obliquity) has major consequences for attempts to reconstruct the tidal dissipation (TD) and dynamical ellipticity (DE) values in the astronomical solution through detailed comparison with the cyclostratigraphic record (see Zeeden et al. 2014). In view of these uncertainties, we preferred to use the La2004 astronomical solution with present day values of TD and DE (written as $La2004_{(1,1)}$) in the present study. Nevertheless, some attempts have been made to reconstruct the TD and DE values based on the detailed cyclostratigraphy in the Upper La Vedova Beach section by Hüsing et al. (2010). In that paper, a TD value of 0.9 results in a good visual fit with the intricate precession-obliquity interference patterns, while in Hüsing (2008) a value of ~ 1.2 is favored as a consequence of the preferred opposite phase relations (the patterns in the insolation target curve essentially becomes mirrored). The latter value is similar to the one that has been inferred from the lower part of the Monte dei Corvi section (Hilgen et al. 2003, Hüsing et al. 2007). Thus the problem of the phase relation has to be solved before TD-DE values can be reliably established. This is critical for comparison with studies that use models of ice volume and mantle convection for reconstructing TD/DE (Morrow et al. 2012).

6.3 Origin of megabeds

6.3.1 Long period astronomical cycles and the MMCO

The magnetobiostratigraphic age constraints indicate that the megabeds are related to the ~100-kyr eccentricity cycle and that the megabed interval (I–VII) corresponds to two successive 405-kyr eccentricity minima and the maximum in between. The limestone part of a cycle (megabed) corresponds to ~100-kyr minimum and the marly interval to ~100-kyr maximum. The expression of megabeds continues up to the top of the section, although these younger cycles are much less indurated and have a more marly appearance. Nevertheless, the true Megabeds I–VII are not well expressed in the $CaCO_3$ content, but in Si/Al (Fig. 5). The indurated character of these beds may thus be explained by an increase in Si rather than in $CaCO_3$ content. Remarkably, the sedimentation rate is significantly reduced in the upper part of the section, which on average has a lower carbonate content. The higher sedimentation rate in the lower part may be related to the increase in Si content observed in the true megabeds (Fig. 5). This Si is likely of biogenic origin and may represent an intermittent decrease in Si content compared to the older Bisciaro Formation that is found stratigraphically ~65 m below the megabeds in coastal cliff sections near Ancona. This unit is composed of marls and limestones with a high volcanoclastic component. Nevertheless, the Si in the Bisciaro Fm is mainly of biogenic origin, although diagenesis has altered the original opal-CT into microcrystalline quartz (Morandi and Tateo 1992). In the world oceans, a positive correlation is often found between sediment accumulation rate and biogenic silica preservation (e.g., De Master et al. 1996, Ragueneau et al. 2000). In these cases, it is inferred that the higher accumulation rate has contributed to enhanced biogenic silica preservation efficiency, but the additional preservation of biogenic silica will also result in higher sedimentation rates.

The expression and amplitude of the small-scale precession related cycles is reduced in the megabed interval. This suggests that this interval may correspond to a minimum in the 2.4 myr eccentricity cycle, when precession amplitude is reduced as a consequence of minimum eccentricity over a prolonged interval of time. However, these minima are reached at 14.2 and 16.6 Ma, thus excluding a link to this very long period eccentricity cycle. Also a relation with the shorter 1.0 myr eccentricity cycle is not evident.

The megabed interval between 16.3 and 15.7 Ma encompasses a minimum (node) in the 1.2 myr obliquity cycle, in which the Mi 2 glacial is placed at around 16 Ma (Fig. 5 in Boulila et al. 2011). However, it is not clear how such an obliquity node and associated, but much shorter, glacial episode may have affected the Mediterranean, as cycle patterns are dominated by the combination of eccentricity and precession, and the top and bottom of the megabed interval are controlled by successive minima of the 405-kyr eccentricity cycle. Also a relation with eustatic sea-level is not evident, as the interval does not coincide with a marked sea-level high- (or low-) stand (Haq et al. 1987, Miller et al. 2005).

Alternatively, one may argue that the megabed interval marks the acme of the MMCO. The MMCO stretches from 17.0 to 15.0 Ma, just before the cooling trend towards the Mi 3b isotope event starts. High-resolution climate proxy records from the open ocean do not reveal that the interval between 15.7 and 16.3 Ma is represented by a climax phase of the MMCO (Holbourn et al. 2007).

6.3.2 Langhian transgression and tectonics

Regional tectonics provide an alternative explanation for the megabed interval, that is not related to any of the very long period eccentricity (or obliquity) cycles. The megabed interval can be related to the so-called Langhian transgression that is widely recorded in the circum-Mediterranean region, including the Paratethys (base Badenian) (e.g., Rögl 1998). This transgression, which is supposed to correspond to the *Praeorbulina* event (Rögl 1998), may have led to a restoration of the connection with the Indian Ocean, resulting in the migration of sub-tropical faunal elements into the Mediterranean-Paratethys area (Rögl 1998).

But what is the age of the Langhian transgression? On Tremiti Islands (Adriatic Sea) this transgression is documented by the sedimentation of shallow marine glauconitic sands, which overlie Eocene limestones with an angular unconformity. The deep marine (hemi-)pelagic sedimentation starts below the Acme_a of *Paragloborotalia siakensis* in the middle of the *S. heteromorphus* Paracme (Di Stefano et al. 2008). The base of *P. siakensis* Acme_a and the *S. heteromorphus* Paracme have estimated ages of 15.48 and 15.74 Ma respectively (Table 3). This suggests that the local onset of marine sedimentation on Tremiti Islands may correspond to the top of the megabed interval at La Vedova. The Langhian transgression supposedly has a tectonic origin (Rögl 1998) and, in case of Tremiti Islands, may reflect deepening of the foreland basin, as a consequence of thrust loading, due to the rapidly advancing orogenic front. In that case, the megabeds at La Vedova may be associated with a phase of tectonic quiescence in the evolving orogen.

During the Neogene, the Apennine system migrated northeastwards with the marly Schlier Formation and turbiditic Marnosa-Arenacea Formation becoming progressively younger towards the NE (e.g., Boccaletti et al. 1990). Tectonic phases are supposed to be reflected in the internal subdivision of the Schlier Formation (e.g., Guerrera et al. 2012). The Marnosa-Arenacea Formation is characterized by the occurrence of marly members deposited on top of the turbidites of the formation, reflecting the – local – end of turbidite deposition and, potentially, orogenic phases of the Apenninic system (Ricci Lucchi and Ori 1985, Guerrera et al. 2012). However, the exact relation of these members with the Schlier succession exposed in the La Vedova section is not clear.

Interestingly, Böhme (2003), studying thermophilic ectothermic vertebrates from the middle Miocene of Central Europe, describes a first phase of enhanced seasonality especially in precipitation between 16.3 and 15.7 Ma, i.e. almost exactly the interval of megabed formation. The author relates this to a tectonic reorganization of the Central Paratethys realm, with subduction of the North European platform and back-arc extension leading to extensive volcanism and the formation of a volcanic belt, which may have affected regional atmospheric circulation. In this particular case, the absence of a relation with long period eccentricity is remarkable as eccentricity modulates the precession amplitude and, hence, has a strong effect on seasonality. The enhanced volcanic activity may also have contributed to the deposition of sediments enriched in biogenic silica in the megabed interval. The presence of radiolarians within Megabed VII (33–35 m) can be regarded as evidence for such a scenario. In addition, washed residues reveal a strong reduction in the amount of foraminifera, suggesting that the biogenic silica producing system was less favorable for foraminifera.

6.4 Langhian GSSP

The Lower La Vedova Beach section is one of two candidate sections for defining the base of the Langhian in the Mediterranean (Iaccarino et al. 2011). The magnetobiostratigraphy, previously published (Turco et al. 2011a) and here revised (Fig. 4), shows that the succession is continuous across the Burdigalian/Langhian boundary. Moreover, the recommended guiding criteria to identify the base of the Langhian – the *Praeorbulina* datum (i.e., *P. glomerosa curva* FO following Turco et al. 2011b) and the top of Chron C5Cn – are both recorded in the section (Iaccarino et al. 2011, Turco et al. 2011a, Turco et al. 2011b, this paper).

Important extra criteria for defining GSSPs in the Neogene are that the section should be astronomically tuned and contain the entire stage in a continuous marine section, representing a unit stratotype for the stage in addition to the GSSP (Hilgen et al. 2006). The tuning of the Lower La Vedova Beach section seems robust at the eccentricity scale, while is less straightforward on the precession scale, as the expression of the basic precession related cycles is not always clear. This is especially evident in the megabed interval that spans the boundary interval, if one prefers to define the boundary close to or at the magnetic reversal associated with the younger end of C5Cn. In addition, the cliffs of La Vedova contain the entire Langhian stage in an essentially continuous and well-tuned succession, from its top as recorded in the La Vedova High Cliff section (Mourik et al. 2010) to its base in the section presented in this paper (Hüsing et al. 2010, Turco et al. 2011a, this paper); the entire La Vedova composite section can thus serve as a unit stratotype for the Langhian. The Lower La Vedova Beach section is in principle suitable to define the GSSP, as it meets the main selection criteria that were set for other deep marine sections selected for defining GSSPs in the Mediterranean (Castradori et al. 1998, Van Couvering et al. 2000, Hilgen et al. 2005). However, at La Vedova the magnetostratigraphy is not of exceptional quality but sufficiently enough to determine the position of the reversals while the biostratigraphy is affected by the moderate to poor preservation of the calcareous plankton. Also the other main candidate section for defining the Langhian GSSP, St. Peter's Pool on Malta, is not ideal as boundary stratotype (Iaccarino et al. 2011). Preservation of the calcareous plankton is much better resulting in an excellent calcareous plankton biostratigraphy, but the magnetostratigraphy is poor.

An alternative option would be to define the GSSP in a deep-sea core. Several (I)ODP sites might be suitable for this purpose: ODP Site 925 (Ceara Rise, Equatorial Atlantic), ODP Site 1264 (Walvis Ridge, South Atlantic), ODP Site 1237 (south eastern Pacific), ODP Site 1146 (South China Sea) and IODP Site U1338 (eastern equatorial Pacific). These sites contain the entire Langhian and are provided with well-preserved calcareous plankton assemblages, stable isotope records, and/or good magnetostratigraphy and astronomical calibration. Moreover, the stable isotope records at Site 1146 and Site U1338 are of exceptional quality, portraying the paleoclimatic history in great detail between 17.0 and 13.6 Ma for Site 1146 and between 16.0 and 13.0 Ma for Site U1338. This picture includes the 405-kyr eccentricity related $\delta^{13}C$ cycles of the Monterey event and the distinct increase in $\delta^{18}O$ associated with the Mi 3b event that reflects a marked increase in Antarctic ice volume (Holbourn et al. 2007, Holbourn et al. 2014).

One can further discuss the desirability of defining a GSSP in a deep-sea core far outside the historical stratotype area of a stage, but with the progress in astronomical tuning, one can equally well argue that GSSPs should be defined in the best possible section or core, as they define global and not regional stages.

7. Conclusions

The magnetobiostratigraphy of the Lower La Vedova Beach section has been improved compared to an earlier publication (Turco et al. 2011a) by taking a previously unnoticed fault into account as a result of the better exposure conditions of the succession.

The magnetic susceptibility and the elemental records of the section have been tuned to eccentricity and precession/insolation, providing astronomical ages for reversal boundaries and calcareous plankton events for the interval between 16.3 and ~ 15.0 Ma.

The tuning to eccentricity seems to be robust (with the individual megabeds corresponding to 100 kyr eccentricity minima), while that to insolation is not always straightforward. The megabed interval (II–VII) shows a relation with the 405 kyr eccentricity cycles, covering two 405-kyr eccentricity minima and the maximum in between, but not with the long period eccentricity cycles.

The megabed interval (II–VII), between ~ 16.3 and 15.7 Ma, is probably linked to regional tectonic activity and the associated circum-Mediterranean Langhian transgression. As such it may represent the last phase of biogenic silica enrichment following the older Bisciaro Formation. This regional tectonic scenario would also explain why this interval is unrelated to any of the very long period eccentricity (or obliquity) cycles, although a strong control by the 405-kyr eccentricity cycle is evident.

The Lower La Vedova Beach section meets key requirements for defining the Langhian GSSP, i.e. the presence of the guiding criteria for its recognition (Top of Chron C5Cn and *Praeorbulina* datum), the astronomical tuning and, together with the Upper La Vedova Beach and the La Vedova High Cliff sections, the presence of the entire Langhian stage in a continuous and tuned succession. However, the magnetobiostratigraphy is not of exceptional quality, the tuning to precession is not always straightforward and the construction of reliable planktonic and benthic isotope records is not possible, due to the moderate to poor preservation of the foraminifera.

Acknowledgements. The authors are very grateful to Ann Holbourn and an anonymous reviewer for their suggestions which improved this work. Giovanna Gianelli is thanked for preparing samples for micropaleontological analysis. This research was financially supported by MIUR (Ministero dell'Istruzione, dell'Università e della Ricerca, Italy) grant (PRIN 2006), the University of Parma (Fil 2012), and the Netherlands Organization for Scientific Research (NWO).

References

Abels, H. A., Hilgen, F. J., Krijgsman, W., Kruk, R. W., Raffi, I., Turco, E., Zachariasse, W. J., 2005. Long-period orbital control on middle Miocene global cooling: integrated stratigraphy and astronomical tuning of the Blue Clay Formation on Malta. Paleoceanography **20**, doi:10.1029/2004PA001129.

Abdul Aziz, H., Di Stefano, A., Foresi, L. M., Hilgen, F. J., Iaccarino, S. M., Kuiper, K. F., Lirer, F., Salvatorini, G., Turco, E., 2008. Integrated stratigraphy and $^{40}Ar/^{39}Ar$ chronology of early Middle Miocene sediments from DSDP Leg 42A, Site 372 (Western Mediterranean). Palaeogeography Palaeoclimatology Palaeoecology **257**, 123–138.

Baksi, A. K., Farrer, E., 1990. Evidence for errors in the geomagnetic polarity time-scale at 17–15 Ma: $^{40}Ar/^{39}Ar$ dating of basalt from the Pacific northwest, USA. Geophysical Research Letters **17**, 1117–1120.

Baksi, A. K., 2012. "New $^{40}Ar/^{39}Ar$ dating of the Grande Ronde lavas, Columbia River Basalts, USA: implications for duration of flood basalt eruption episodes" by Barry et al. (2010) – Discussion. Lithos **146–147**, 293–299.

Barry, T. L., Self, S., Kelley, S. P., Reidel, S., Hooper, P., Widdowson, M., 2010. New $^{40}Ar/^{39}Ar$ dating of the Grande Ronde lavas, Columbia River Basalts, USA: implications for duration of flood basalt eruption episodes. Lithos **118**, 213–222.

Barry, T.L., Self, S., Kelley, S.P., Reidel, S., Hooper, P., Widdowson, M., 2012. Response to Baksi, A., 2012, 'New $^{40}Ar/^{39}Ar$ dating of the Grande Ronde lavas, Columbia river basalts, USA: Implications for duration of flood basalt eruption episodes' by Barry et al., 2010 – discussion'. Lithos **146–147**, 300–303.

Barry, T.L., Kelley, S.P., Reidel, S.P., Camp, V.E., Self, S., Jarboe, N.A., Duncan, R.A., Renne, P.R., 2013. Eruption Chronology of the Columbia River Basalt Group. Geological Society of America, Special Paper **497**, 45–66.

Boccaletti, M., Calamita, F., Deiana, G., Gelati, R., Massari, F., Moratti, G., Ricci Lucchi, F., 1990. Migrating foredeep-thrust belt system in the Northern Apennines and Southern Alps. Palaeogeography Palaeoclimatology Palaeoecology **77**, 3–14.

Böhme, M., 2003. The Miocene climatic optimum: Evidence from ectothermic vertebrates of central Europe. Palaeogeography, Palaeoclimatology, Palaeoecology **195**, 389–401.

Bosmans, J.H.C., Hilgen, F.J., Tuenter, E., Lourens, L.J., 2015. Obliquity forcing of low-latitude climate. Climate of Past **11**, 1335–1346.

Boulila, S., Galbrun, B., Miller, K.G., Pekar, S.F., Browning, J.V., Laskar, J., Wright, J.D., 2011. On the origin of Cenozoic and Mesozoic "third-order" eustatic sequences. Earth-Science Reviews **109**, 94–112.

Calvert, S.E., Fontugne, M.R., 2001. On the late Pleistocene-Holocene sapropel record of climatic and oceanographic variability in the eastern Mediterranean. Paleoceanography **16**, 78–94.

Castradori, D., Rio, D., Hilgen, F.J., Lourens, L.J., 1998. The Global Standard Stratotype-section and Point (GSSP) of the Piacenzian Stage (Middle Pliocene). Episodes **21**, 88–93.

Chen, J., Zhisheng, A., Head, J., 1999. Variation of Rb/Sr Ratios in the Loess-Paleosol Sequences of Central China during the Last 130,000 Years and Their Implication for Monsoon Paleoclimatology. Quaternary Research **51**, 215–219.

Deino, A., Channell, J., Coccioni, R., De Grandis, G., De Paolo, D.J., Fornaciari, E., Emmanuel, L., Laurenzi, M.A., Montanari, A., Rio, D., Renard, M., 1997. Integrated stratigraphy of the upper Burdigalian -lower Langhian section at Moria (Marche Region, Italy). In: Montanari, A., Odin, G.S., Coccioni, R. (Eds.), Miocene stratigraphy: An integrated approach. Developments in Palaeontology and Stratigraphy **15**, Elsevier, Amsterdam, p. 315–341.

De Master, D.J., Ragueneau, O., Nittrouer, C.A., 1996. Preservation efficiencies and accumulation rates for biogenic silica and organic C, N, and P in high-latitude sediments: The Ross Sea. Journal Of Geophysical Research **101**, C8, 18.501–18.518.

De Visser, J.P., Ebbing, J.H.J., Gudjonsson, L., Hilgen, F.J., Jorissen, F.J., Verhallen, P.J.J.M., Zevenboom, D., 1989. The origin of rhythmic bedding in the Pliocene Trubi Formation of Sicily, southern Italy. Palaeogeography, Palaeoclimatology, Palaeoecology **69**, 45–66.

Di Stefano, A., Foresi, L.M., Lirer, F., Iaccarino, S.M., Turco, E., Amore, F.O., Mazzei, R., Morabito, S., Salvatorini, G., Abdul Aziz, H.A., 2008. Calcareous plankton high resolution bio-magnetostratigraphy for the Langhian of the Mediterranean area. Rivista Italiana di Paleontologia e Stratigrafia **11**, 51–76.

Ellwood, B.B., Crick, R.E., El Hassani, A., Benoist, S.L., Young, R.H., 2000. Magnetosusceptibility event and cyclostratigraphy method applied to marine rocks; detrital input versus carbonate productivity. Geology **28**, 1135–1138.

Foresi, L.M., Verducci, M., Baldassini, N., Lirer, F., Mazzei, R., Salvatorini, G., Ferraro, L., Da Prato, S., 2011. Integrated stratigraphy of St. Peter's Pool section (Malta): new age for the Upper Globigerina Limestone Member and progress towards the Langhian GSSP. Stratigraphy **8**, 125–143.

Fornaciari, E., Di Stefano, A., Rio, D., Negri, A., 1996. Middle Miocene quantitative calcareous nannofossil biostratigraphy in the Mediterranean region. Micropaleontology **42**, 37–63.

Goddard, E.N., Trask, P.D., De Ford, R.K., Rowe, O.N., Singewald, J.T., Overbeck, R.M., 1963. Rock Color Chart. Boulder: Geological Society of America.

Grant, K.M., Grimm, R., Mikolajewicz, U., Marino, G., Ziegler, M., Rohling, E.J., 2016. The timing of Mediterranean sapropel deposition relative to insolation, sea-level and African monsoon changes. Quaternary Science Reviews **140**, 125–141.

Guerrera, F., Tramontana, M., Donatelli, U., Serrano, F., 2012. Space/time tectono-sedimentary evolution of the Umbria–Romagna–Marche Miocene basin (northern Apennines, Italy): A foredeep model. Swiss Journal of Geosciences **105**, 325–341.

Haq, B.U., Hardenbol, J., Vail, P.R., 1987. Chronology of fluctuating sea levels since the Triassic. Science **235**, 1156–1167.

Hay, W.W., 1996. Tectonics and climate. Geologische Rundschau **85**, 409–437.

Hay, W.W., 1998. Detrital sediment fluxes from continents to oceans. Chemical Geology **145**, 287–323.

Hilgen, F.J., 1991. Extension of the astronomically calibrated (polarity) time scale to the Miocene/Pliocene boundary. Earth and Planetary Science Letters **107**, 349–368.

Hilgen, F., Abdul Aziz, H., Bice, D., Iaccarino, S., Krijgsman, W., Kuiper, K., Montanari, A., Raffi, I., Turco, E., Zachariasse, W.-J., 2005. The global boundary stratotype section and point (GSSP) of the Tortonian stage (upper Miocene) at Monte dei Corvi.Episodes **28**, 6–17.

Hilgen, F.J., Abdul Aziz, H.A., Krijgsman, W., Raffi, I., Turco, E., 2003. Integrated stratigraphy and astronomical tuning of the Serravallian and lower Tortonian at Monte dei Corvi (Middle–Upper Miocene, northern Italy). Palaeogeography Palaeoclimatology Palaeoecology **199**, 229–264.

Hilgen, F., Brinkhuis, H., Zachariasse, W.-J., 2006. Unit stratotypes for global stages: the Neogene perspective. Earth-Science Reviews **74**, 113–125.

Hilgen, F.J., Lourens, L.J., van Dam, J.A., 2012. The Neogene Period. In: Gradstein, F., Ogg, J., Schmitz, M., Ogg,

G. (Eds.), The Geological Time Scale 2012. Elsevier, Amsterdam, p. 923–978.

Holbourn, A., Kuhnt, W., Schulz, M., Erlenkeuser, H., 2005. Impacts of orbital forcing and atmospheric carbon dioxide on Miocene ice-sheet expansion. Nature **438**, 483–487.

Holbourn, A., Kuhnt, W., Schulz, M., Flores, J.-A., Andersen, N., 2007. Orbitally-paced climate evolution during the middle Miocene "Monterey" carbon-isotope excursion. Earth and Planetary Science Letters **261**, 534–550.

Holbourn, A., Kuhnt, W., Clemens, S., Prell, W., Andersen, N., 2013. Middle to late Miocene stepwise climate cooling: Evidence from a high-resolution deep water isotope curve spanning 8 million years. Paleoceanography **28**, 688–699.

Holbourn, A., Kuhnt, W., Lyle, M., Schneider, L., Romero, O., Andersen, 2014. Middle Miocene climate cooling linked to intensification of eastern equatorial Pacific upwelling. Geology **42**, 19–22.

Hüsing, S. K., 2008. Astrochronology of the Mediterranean Miocene: Linking palaeoenvironmental changes to gateway dynamics. PhD thesis, Geologica ultraiectina, Utrecht University, 295 pp.

Hüsing, S. K., Hilgen, F. J., Abdul Aziz, H., Krijgsman, W., 2007. Completing the Neogene geological time scale between 8.5 and 12.5 Ma. Earth and Planetary Science Letters **253**, 340–358.

Hüsing, S. K., Hilgen, F. J., Kuiper, K. F., Krijgsman, W., Turco, E., Cascella, A., Wilson, D., 2010. Astrochronology of the Mediterranean Langhian between 15.29 and 14.17 Ma. Earth and Planetary Science Letters **290**, 254–269.

Iaccarino, S., 1985. Mediterranean Miocene and Pliocene planktic foraminifera. In: Bolli, H. M., Saunders, J. B., Perch-Nielsen, K. (Eds.), Plankton stratigraphy, Cambridge University Press, Cambridge, p. 283–314.

Iaccarino, S., Salvatorini, G., 1982. A framework of planktonic foraminifera biostratigraphy for early Miocene to Late Pliocene Mediterranean area. Paleontologia Stratigrafica ed Evoluzione **2**, 115–125.

Iaccarino, S., Di Stefano, A., Foresi, L. M., Turco, E., Baldassini, N., Cascella, A., Da Prato S., Ferraro, L., Gennari, R., Hilgen, F. J., Lirer, F., Maniscalco, R., Mazzei, R., Riforgiato, F., Russo, B., Sagnotti, L., Salvatorini, G., Speranza, F., Verducci, M., 2011. High-resolution integrated stratigraphy of the upper Burdigalian–lower Langhian in the Mediterranean: the Langhian historical stratotype and new candidate sections for defining its GSSP. Stratigraphy **8**, 199–215.

Jarboe, N. A., Coe, R. S., Renne, P. R., Glen, J. M. G., Mankinen, E. A., 2008. Quickly erupted volcanic sections of the Steens Basalt, Columbia River Basalt Group: Secular variation, tectonic rotation, and the Steens Mountain reversal: Geochemistry Geophysics. Geosystems **9**, doi: 10.1029/2008GC002067.

Jarboe, N. A., Coe, R. S., Renne, P. R., Glen, J. M. G., 2010. The age of the Steens reversal and the Columbia River Basalt Group. Chemical Geology **274**, 158–168.

Kuiper, K. F., Deino, A., Hilgen, F. J., Krijgsman, W., Renne, P. R., Wijbrans, J. R., 2008. Synchronizing rock clocks of Earth history. Science **320**, 500–504.

Laskar, J., Robutel, P., Joutel, F., Gastineau, M., Correia, A. C. M., Levrard, B., 2004. A long term numerical solution for the insolation quantities of the Earth. Astronomy and Astrophysics **428**, 261–285.

Lourens, L.J., Antonarakou, A., Hilgen, F.J., Van Hoof, A. A. M., Vergnaud-Grazzini, C., Zachariasse, W. J., 1996. Evaluation of the Plio-Pleistocene astronomical timescale. Paleoceanography **11**, 391–413.

Mader, D., Cleaveland, L., Bice, D., Montanari, A., Koeberl, C., 2004. High-resolution cyclostratigraphic analysis of multiple climate proxies from a short Langhian pelagic succession in the Conero Riviera, Ancona (Italy). Palaeogeography Palaeoclimatology Palaeoecology **211**, 325–344.

Miller, K. G., Wright, J. D., Fairbanks, R. G., 1991. Unlocking the ice house: Oligocene –Miocene oxygen isotopes, eustacy and margin erosion. Journal of Geophyical. Research **96**, 6829–6848.

Miller, K. G., Kominz, M. A., Browning, J. V., Wright, J. D., Mountain, G.S., Katz, M.E., Sugarman, P.J., Cramer, B.S., Christie-Blick, N., Pekar, S.F., 2005. The phanerozoic record of global sea-level change. Science **310**, 1293–1298.

Montanari, A., Beaudoin, B., Chan, L.S., Coccioni, R., Deino, A., De Paolo, D. J., Emmanuel, L., Fornaciari, E., Kruge, M., Lundblad, S., Mozzato, C., Portier, E., Renard, M., Rio, D., Sandroni, P., Stankiewicz, A., 1997. Integrated stratigraphy of the Middle and Upper Miocene pelagic sequence of the Conero Riviera (Marche region, Italy). In: Montanari, A., Odin, G. S., Coccioni, R. (Eds.), Miocene Stratigraphy: An Integrated Approach. Developments in Palaeontology and Stratigraphy **15**, Elsevier, Amsterdam, p. 409–450.

Morandi, N., Tateo, F., 1992. Mineralogy of pelitic "Bisciaro" & "Schlier" sediments in S. Croce and Moria sections (Marche region, Italy). Mineralogica Petrographica Acta **35**, 235–255.

Morrow, E., Mitrovica, J., Forte, A., Glišović, P., Huybers, P., 2012. An enigma in estimates of the Earth's dynamic ellipticity. Geophysical Journal International **191**, 1129–1134, doi:10.1111/j.1365-246X.2012.05703.x.

Mourik, A.A., Bijkerk, J.F., Cascella, A., Hüsing, S.K., Hilgen, F. J., Lourens, L. J., Turco, E., 2010. Astronomical tuning of the La Vedova high cliff section (Ancona, Italy) – implications of the Middle Miocene climate transition for Mediterranean sapropel formation. Earth and Planetary Science Letters **297**, 249–261.

Nijenhuis, I.A., Schenau, S.J., Van der Weijden, C.H., Hilgen, F. J., Lourens, L. J., Zachariasse, W. J., 1996. On the origin of upper Miocene sapropelites: A case study from the Faneromeni section, Crete (Greece). Paleoceanography **11**, 633–645.

Paillard, D., Labeyrie, L., Yiou, P., 1996. Macintosh program performs time-series analysis. Eos **77**, 379.

Poulton, S.W., Raiswell, R., 2002. The low-temperature geochemical cycle of iron: from continental fluxes to marine sediment deposition. American Journal of Science **302**, 774–805.

Ragueneau, O., Tréguer, P., Leynaert, A., Anderson, R.F., Brzezinski, M.A., DeMaster, D.J., Dugdale, R.C., Dymond, J., Fischer, G., François, R., Heinze, C., Maier-Reimer, E., Martin-Jézéquel, V., Nelson, D.M., Quéguiner, B., 2000. A review of the Si cycle in the modern ocean: Recent progress and missing gaps in the application of biogenic opal as a paleoproductivity proxy. Global and Planetary Change **26**, 317–365.

Ricci Lucchi, F., Ori, G.G., 1985. Field excursion D: synorogenic deposits of a migrating basin system in the NW Adriatic Foreland. In: Allen, P.H., Homewood, P., Williams, G. (Eds.), Excursion guidebook. Foreland Basins Symposium, Fribourg, p. 137–176.

Rögl, F., 1998. Palaeogeographic considerations for Mediterranean and Paratethys Seaways (Oligocene to Miocene). Annalen des Naturhistorischen Museums in Wien **99A**: 279–310.

Sandroni, P., 1985. Rilevamento geologico al 1:10.000 e litostratigrafia di alcuni sezioni dello Schlier nel bacino marchigiano esterno e studio mineralogico e petrografico di una sezione ricostruita nell'anticlinale del Conero. Unpubl. PhD Thesis, University of Urbino, 188 pp.

Schenau, S.J., Antonarakou, A., Hilgen, F.J., Lourens, L.J., Nijenhuis, I.A., van der Weijden, C.H., Zachariasse, W.J., 1999. Organic-rich layers in the Metochia section (Gavdos, Greece): evidence for a single mechanism of sapropel formation during the past 10 My. Marine Geology **153**, 117–135.

Sprovieri, R., 1992. Mediterranean Pliocene biochronology: An high resolution record based on quantitative planktonic foraminifera distribution. Rivista Italiana di Paleontologia e Stratigrafia **98**, 61–100.

Sprovieri, M., Caruso, A., Foresi, L.M., Bellanca, A., Neri, R., Mazzola, S., Sprovieri, R., 2002. Astronomical calibration of the upper Langhian/lower Serravallian record of Ras il-Pellegrin section (Malta island, central Mediterranean). Rivista Italiana di Paleontologia e Stratigrafia **108**, 183–193.

Sprovieri, R., Sprovieri, M., Caruso, A., Pelosi, N., Bonomo, S., Ferraro, L., 2006. Astronomic forcing on the planktonic foraminifera assemblage in the Piacenzian Punta Piccola section (southern Italy). Paleoceanography **21**, doi:10.1029/2006PA001268.

Tian, J., Yang, M., Lyle, M.W., Wilkens, R., Shackford, J.K., 2013. Obliquity and long eccentricity pacing of the Middle Miocene climate transition. Geochemistry Geophysics Geosystems **14**, 1740–1755.

Torrence, C., Compo, G.P., 1998. A practical guide to wavelet analysis. Bulletin of American Meteorological Society **79**, 61–78.

Turco, E., Cascella, A., Gennari, R., Hilgen, F.J., Iaccarino, S.M., Sagnotti, L., 2011a. Integrated stratigraphy of the La Vedova section (Conero Riviera, Italy) and implications for the Burdigalian/Langhian boundary. Stratigraphy **8**, 89–110.

Turco, E., Iaccarino, S.M., Foresi, L., Salvatorini, G., Riforgiato, F., Verducci, M., 2011b. Revisiting the taxonomy of the intermediate stages in the *Globigerinoides – Praeorbulina* lineage. Stratigraphy **8**, 163–187.

Van Couvering, J.A., Castradori, D., Cita, M.B., Hilgen, F.J., Rio, D., 2000. The base of the Zanclean Stage and of the Pliocene Series. Episodes **23**, 179–187.

Van Os, B.J.H., Lourens, H.J., Hilgen, F.J., De Lange, G.J., Beaufort, L., 1994. The formation of Pliocene sapropels and carbonate cycles in the Mediterranean: Diagenesis, dilution, and productivity. Paleoceanography **9**, 601–617.

Vincent, E., Berger, W.H., 1985. Carbon dioxide and polar cooling in the Miocene: the Monterey hypothesis. In: Broecker, W.S., Sundquist, E.T. (Eds.), The Carbon Cycle and Atmospheric CO_2: Natural Variations Archean to Present. Geophysical Monograph Series, vol. **32**. AGU, Washington, DC, p. 455–468.

Wehausen, R., Brumsack, H.-J., 2000. Chemical cycles in Pliocene sapropel-bearing and sapropel-barren eastern Mediterranean sediments. Palaeogeography Palaeoclimatology Palaeoecology **158**, 325–352.

Woodruff, F., Savin, S., 1991. Mid-Miocene isotope stratigraphy in the deep sea: high resolution correlations, paleoclimatic cycles, and sediment preservation. Paleoceanography **6**, 755–806.

Zeeden, C., Hilgen, F.J., Hüsing, S.K., Lourens, L.J. 2014. The Miocene astronomical time scale 9–12 Ma: New constraints on tidal dissipation and their implications for paleoclimatic investigations. Paleoceanography **29**, 296–307.

Ziegler, M., Tuenter, E., Lourens, L.J., 2010. The precession phase of the boreal summer monsoon as viewed from the eastern Mediterranean (ODP Site 968). Quaternary Science Reviews **29**, 1481–1490.

Zhisheng, A., Kutzbach, J.E., Prell, W.L., Porter, S.C., 2001. Evolution of Asian monsoons and phased uplift of the Himalaya-Tibetan plateau since Late Miocene times. Nature **411**, 62–66.

Manuscript received: November 29, 2015
Revised version accepted: June 24, 2016

The pdf version of this paper includes an electronic supplement

Please save the electronic supplement contained in this pdf-file by clicking the blue frame above. After saving rename the file extension to .zip (for security reasons Adobe does not allow to embed .exe, .zip, .rar etc. files).

Table of contents – Electronic Supplementary Material (ESM)

Supplementary material A
Supplementary material A includes information on the succession of the Lower La Vedova section regarding: i) details of the alternation of more indurated and prominent limestones (megabed) and more marly intervals, from the top of the section to Megabed V (Fig. A1a–c); ii) different outcrop conditions of Megabeds VII and VI in 2008, when the section was sampled, and in summer 2012 after winter storms (Fig. A1d). Moreover, the internal pattern of the megabeds in the revised composite section of the Lower La Vedova Beach section is compared with that of the 7 megabeds very well exposed along the cliffs close to Ancona (Fig. A2).

Supplementary material B
Supplementary material B presents the results of the Principal Component Analysis carried out on the geochemical elements normalized with Al. The component matrix for the three extracted components (PC1, PC2, PC3) is shown in Table B1 and their score plots are plotted next to the lithological column of the Lower La Vedova section in Figure B1.

Supplementary material C
Supplementary material C presents an alternative tuning to precession/insolation based on the opposite phase relation of limestone beds (and associated Ca-maxima) with precession and insolation cycles (Fig. C1).